PFC/JA-86-36

Energy Confinement Studies of Lower Hybrid Current Driven Plasmas in the Alcator C Tokamak

Y. Takase, P. Bonoli, S. Knowlton,
M. Porkolab, S. Texter, C. Fiore, S. McCool*,
S. McDermott, J. Terry

June 1986

Plasma Fusion Center
Massachusetts Institute of Technology
Cambridge, MA 02139

*Present Address: University of Texas, Austin, Texas, U.S.A.

Submitted for Publication in: Nuclear Fusion

ENERGY CONFINEMENT STUDIES OF LOWER HYBRID CURRENT DRIVEN PLASMAS IN THE ALCATOR C TOKAMAK

Y. TAKASE, P. BONOLI, S. KNOWLTON,

M. PORKOLAB, S. TEXTER,

C. FIORE, S. McCOOL, *

S. McDERMOTT, J. TERRY

Plasma Fusion Center,

Massachusetts Institute of Technology,

Cambridge, Massachusetts

United States of America

ABSTRACT. Energy confinement is studied in lower hybrid current driven (LHCD) plasmas in Alcator C in the density range $\overline{n}_e = (1\text{–}8) \times 10^{13}\,\mathrm{cm}^{-3}$. In LHCD plasmas, the stored energy in the electron tail W^{tail} can be a significant fraction of the total stored energy W^{tot}, especially at lower densities. At sufficiently low densities, the energy confinement time of the high energy electrons is expected to become shorter than their collisional energy slowing down time, and direct energy losses from the electron tail can become important in the overall power balance. The global energy confinement time, defined as $\tau_E^{tot} \equiv W^{tot}/P_{tot}$, is found to be comparable to or exceed that in ohmically heated (OH) plasmas at low densities $\overline{n}_e \lesssim 3 \times 10^{13}\,\mathrm{cm}^{-3}$, where a steady state current can be maintained with

* present address : University of Texas, Austin, Texas, U.S.A.

relatively low rf power. However, at higher densities where substantially more rf power is needed (relative to the ohmic power required to maintain a similar plasma), a deterioration of τ_E^{tot} relative to ohmic confinement, similar to that predicted by the neutral beam heated L-mode scaling, is observed. Theoretical modeling with the aid of a ray tracing-Fokker Planck-transport code suggests that the deteriorated confinement in this high density, high power regime may be attributed to an enhanced bulk electron thermal diffusivity. In a combined OH-LHCD plasma, a value of τ_E^{tot} greater than the ohmic value is obtained as long as the applied rf power does not significantly exceed the ohmic power.

1. INTRODUCTION

Energy confinement in auxiliary heated tokamak plasmas has received considerable attention in the past few years. Although energy confinement in neutral beam heated plasmas has been studied extensively and is well documented[1], the study of energy confinement in intensely rf (radio frequency) wave heated plasmas has only recently begun and relatively little information is available at present[2, 3]. We report here the results of energy confinement studies performed during lower hybrid current drive (LHCD) on the Alcator C tokamak[4,5]. In particular, we have been able to study energy confinement in tokamak plasmas which are maintained purely by non-inductive means ($P_{AUX}/P_{OH} = \infty$) using LHCD. We shall concentrate mainly on energy confinement in such purely rf maintained plasmas in the present paper. Results from combined OH-LHCD plasmas are also discussed.

LHCD experiments were performed in hydrogen plasmas in the Alcator C tokamak with parameters in the range B_T = 7–11 T, I_p = 100–200 kA, $\bar{n}_e$ = (1–8) $\times 10^{13}$ cm^{-3}. Molybdenum limiters defined the plasma with major and minor radii of $R_0 = 64$ cm and $a = 16.5$ cm, respectively. Typical values of Z_{eff} were 1.5–2 during the present set of experiments. A typical LHCD shot and a similar OH shot are shown in Fig. 1. The ohmic power was removed by open-circuiting the OH primary circuit after plasma formation. Upon application of rf power, the surface loop voltage drops to zero within 20–30ms, and thereafter the plasma is maintained and heated entirely by rf power alone. Utilizing three 4×4 waveguide arrays, up to 1.5MW of rf power at 4.6GHz was injected. A relative waveguide phasing of $\Delta\phi = 90°$ between adjacent waveguides was used to launch a spectrum of waves traveling predominantly in the direction of the average electron drift velocity.

The plan of the paper is as follows : A discussion of power balance during

LHCD is presented in Sec. 2. The analysis method is also outlined. In Sec. 3 the scaling of energy confinement time in LHCD plasmas is discussed and compared with that of OH plasmas, and also with a neutral beam scaling. In Sec. 4 the transition from purely OH to purely LHCD plasmas is discussed together with the effects of finite inductive electric field. Results of code modeling of these experiments are presented and discussed in Sec. 5. Finally, in Sec. 6 the conclusions are given.

2. POWER BALANCE DURING LHCD

A schematic diagram of the power balance model applicable to LHCD and LH electron heating is shown in Fig. 2. A large fraction of the rf power injected into the plasma, $P_{abs} = \eta_{abs} P_{rf}$, is expected to be absorbed via electron Landau damping by tail electrons resonant with the wave phase velocity. Since the tail electrons are not perfectly confined, the power collisionally dissipated on the bulk electrons, P_d, is only some fraction of this absorbed power, depending on the relative magnitudes of the collisional slowing down time and the electron tail confinement time. The remainder of the absorbed power is lost directly from the tail before slowing down on the bulk, either by radiation or by transport. The presence of such loss mechanisms are evidenced by large increases in plasma hard X-ray Bremsstrahlung radiation, superthermal electron cyclotron emission, and limiter hard X-rays during the LHCD phase compared to the OH phase. The limiter hard X-ray signal is shown in Fig. 1. The transport loss to the limiters is believed to be the dominant direct tail loss mechanism in Alcator C LHCD plasmas[6]. Bulk ions are heated through collisional equilibration with electrons. For simplicity, in the present analysis of overall power balance, we shall not separate out the bulk ion transport from the bulk electron transport.

We can define the bulk energy confinement time $\tau_E^{bulk} \equiv W^{bulk}/P_d$, which

characterizes the confinement property of the bulk plasma. Here, $W^{bulk} = W_e^{bulk} + W_i^{bulk}$ is the sum of the stored energies of the bulk electrons and ions. However, since P_d is a difficult quantity to measure experimentally, in the present paper we shall mainly use the global energy confinement time defined as $\tau_E^{tot} \equiv W^{tot}/P_{tot}$, where $W^{tot} \equiv W^{bulk} + W^{tail}$, $P_{tot} \equiv P_{rf} + P_{OH}$ ($= P_{rf}$ in purely rf driven plasmas) for our scaling studies. We have used P_{rf} in the denominator instead of P_{abs} by assuming $P_{abs} \simeq P_{rf}$ ($\eta_{abs} \simeq 1$) since the absorption efficiency η_{abs} is not measured experimentally. This gives a lower limit on τ_E^{tot}. As will be discussed in Sec. 5, according to our code modeling[7] a nearly complete absorption by electron Landau damping, $\eta_{abs} > 0.8$ (more typically $\eta_{abs} > 0.9$), is necessary to match the experimentally obtained current drive efficiency. The radiated power, which is not a significant fraction of the input power except possibly at very low densities $\overline{n}_e < 3 \times 10^{13}\,\mathrm{cm}^{-3}$, has not been subtracted out. Because of the non-neglible amounts of energy stored in the tail, and the possibility of direct radial loss of a portion of this energy from the tail, the quantity defined as $\tau_E' \equiv W^{bulk}/P_{tot}$ gives an underestimate for the true bulk energy confinement time, τ_E^{bulk}. The scaling of τ_E' will also be shown, but it should not be taken to represent the bulk energy confinement time, τ_E^{bulk}. We note that if the energy slowing down time of the high energy electrons were sufficiently shorter than the electron tail energy confinement time, as would be the case in larger machines with better electron tail confinement, or at higher densities, we would expect that most of the absorbed power would be utilized in bulk heating so that $P_d \simeq P_{abs}$. Such is also the situation in LH heating studies, performed at higher densities in Alcator C[8].

The bulk stored energy, W^{bulk}, was obtained from standard profile measurements (5-channel FIR interferometer, 5-channel Thomson scattering system, vertically scanning charge exchange analyzer). For the purpose of analysis, the electron

temperature measurements are fitted to a gaussian profile with width a_{Te}, such that $T_e(r) = T_e(0)\exp(-r^2/a_{Te}^2)$. The ion temperature profile, measured at $B = 8\,\mathrm{T}$, $I_p = 140\,\mathrm{kA}$, and $\overline{n}_e = 6\times10^{13}\,\mathrm{cm}^{-3}$, was somewhat broader (10–20% in the profile width) than the electron temperature profile. Since only the central ion temperature measurements were available under other conditions, the ion temperature profile width was scaled with the electron temperature profile width. The density profiles of both OH and LHCD plasmas had a typical peak-to-average ratio of 1.5 in this "low density" ($\overline{n}_e < 1\times10^{14}\,\mathrm{cm}^{-3}$) regime, corresponding to a parabolic profile.

The time evolution of the central electron temperature, as measured by Thomson scattering, is shown in Fig. 3 for the LHCD and OH plasmas illustrated in Fig. 1. Both the values of the temperature and the time histories for the two cases are similar under these conditions, and both follow approximately the evolution of the plasma current. However, they can be different under some conditions. For example, the electron temperature profiles for LHCD and OH plasmas at a lower current ($I_p = 110\,\mathrm{kA}$, $q = 15.5$) are shown in Fig. 4. The temperature profiles are extremely peaked in these low current plasmas. The LHCD plasma is hotter than the OH plasma in this particular case.

The stored energy of the electron tail, W^{tail}, was estimated from $\beta_p + \ell_i/2$ obtained from the vertical field measurement using Shafranov's equilibrium condition[9]

$$B_v = -\frac{\mu_0 I_p}{4\pi R}\left(\ln\frac{8R}{a} + \beta_p + \frac{\ell_i}{2} - \frac{3}{2}\right).$$

Here $\beta_p \equiv \mu_0[\langle P_\parallel(r)\rangle + \langle P_\perp(r)\rangle]/B_p(a)^2$ and $\ell_i/2 \equiv \langle B_p(r)^2\rangle / B_p(a)^2$, where the brackets denote volume average, $P_\parallel$ and $P_\perp$ are the parallel and perpendicular elements of the relativistic pressure tensor[10], and B_p is the poloidal magnetic

field. Based on the electron tail distribution function inferred from angular plasma hard X-ray measurements[6], we estimate $P_{\parallel}^{tail}/P_{\perp}^{tail} \simeq 2$ for the tail component.

The value of $\beta_p + \ell_i/2$ obtained from the equilibrium field measurement is shown as a function of plasma current in Fig. 5 for both LHCD and OH plasmas at constant B_T and $\overline{n}_e$. The thermal contribution to β_p, denoted as β_p^{bulk}, is determined from the temperature and density profile analysis, and the results are also displayed in Fig. 5. The absolute value of $\beta_p + \ell_i/2$ is uncertain, but the relative error of the measurement is approximately 0.05. Because of the uncertainty in the absolute value of $\beta_p + \ell_i/2$, only the relative measurement is used to determine the tail contribution to β_p. Since β_p^{bulk} is similar for both LHCD and OH, the difference between $\beta_p + \ell_i/2$ for the two cases would correspond to β_p^{tail} for the LHCD case if $\ell_i/2$ for the two cases were similar.

A rather large uncertainty in determining $\ell_i/2$ experimentally (uncertain by up to 0.1) introduces a corresponding uncertainty in the tail stored energy W^{tail}. In LHCD plasmas, the current density profile is not necessarily related to the electron temperature profile through resistivity. Recent measurements by the ASDEX group[11] indicate that the current density profiles of LHCD plasmas are broader than that obtained by assuming $j(r) \propto T_e(r)^{3/2}$. Such a result is also predicted by our numerical modeling. The plasma hard X-ray (30–500keV) profile, which reflects the profile of current carrying high energy electrons, was also consistently broader than the electron temperature profile[12], and its scaling with plasma parameters was similar to that of the electron temperature profile. Although $\ell_i/2$ could not be determined absolutely from the hard X-ray profiles, they can be used as a qualitative measure of how the current density profile changes with plasma parameters. The dependencies of the central electron temperature and its gaussian profile width on plasma current are shown in Fig. 6 for the case shown in Fig. 5. The widths

of the plasma hard X-ray gaussian profiles at different energies, obtained using a vertically viewing eight detector array, are shown in Fig. 7 as functions of plasma current. These observations lead us to calculate an upper limit on $\ell_i/2$ using the relationship $j(r) \propto T_e(r)^{3/2}$. We have chosen to use the relationship $j(r) \propto T_e(r)$ to calculate a lower limit on $\ell_i/2$. Since the bulk electron heating power is provided solely by the collisional slowing down of the current carrying energetic electrons in purely rf-driven LHCD plasmas, the bulk electron temperature profile is expected to be broader than the slowing down power profile, $P_d(r)$, which would be well represented by $j(r)$ if the shape of the tail distribution function f_e^{tail} were independent of minor radius. However, this lower limit is not a strict limit. If, as suggested by the plasma hard X-ray data shown in Fig. 7, the tail distribution function were more energetic at larger minor radii, a heating profile $P_d(r)$ which is narrower than $j(r)$ is possible, because P_d is weighted toward lower energy electrons whereas j is weighted toward higher energy electrons. If in fact $j(r)$ were broader than $T_e(r)$, β_p^{tail} would become larger than the present estimate. The error bars on $\beta_p^{bulk} + \ell_i/2$ for the LHCD case shown in Fig. 5 reflect the uncertainty in the determination of $\ell_i/2$.

In addition to the equilibrium field measurements, at a density of $\overline{n}_e = 3 \times 10^{13}\,\mathrm{cm}^{-3}$ and a current of $I_p = 140\,\mathrm{kA}$, it has been possible to infer the electron tail distribution function $f_e^{tail}(p_\parallel, p_\perp)$ from the data obtained with plasma hard X-ray detector arrays[6]. Hard X-ray emission from high energy electrons are collected at five different angles with respect to the magnetic field. Together with the spatial profile data obtained from the eight detector vertical array, the two-dimensional electron tail distribution function, $f_e^{tail}(p_\parallel, p_\perp)$ is reconstructed, exploiting the anisotopic nature of the Bremsstrahlung radiation pattern[13]. We note that the spatial structure of the electron tail distribution function could not be

determined by this method, and the reconstructed distribution function represents a spatial average. Using this distribution function, the stored energy in the electron tail W^{tail}, the collisionally dissipated power on the bulk plasma P_d, and radiated powers (Bremsstrahlung power P_B and cyclotron power P_c) have been estimated. An example of power balance for a typical LHCD plasma, obtained using this technique, is summarized in Table I. For the present case, $W^{tail} \simeq 1.4\,\mathrm{kJ}$, $P_d \simeq 150\,\mathrm{kW}$, $P_c \simeq 16\,\mathrm{kW}$, and $P_B \simeq 0.01\,\mathrm{kW}$[6]. The tail stored energy calculated from the equilibrium measurements, $W^{tail} = 1.3 \pm 0.5\,\mathrm{kJ}$, agree within experimental uncertainties with that deduced from the hard X-ray measurements, $W^{tail} = 1.4 \pm 0.3\,\mathrm{kJ}$. It is seen that W^{tail} is comparable to (or even larger than) W^{bulk}, and that the radial power loss from the tail, $P_l \simeq P_{rf} - P_d - P_c - P_B \simeq 134\,\mathrm{kW}$, represents a significant fraction of the input rf power $P_{rf} = 300\,\mathrm{kW}$ according to the present analysis. However, we note that there is a large uncertainty in the determination of P_d (and therefore, on P_l) because of its sensitivity to the low energy part of the distribution function, which is not well diagnosed by the hard X-ray emission technique. For this case $\tau_E^{tot} \simeq 8\,\mathrm{ms}$ (based on hard X-ray measurements), $\tau_E^{tot} \simeq 7\,\mathrm{ms}$ (based on $\beta_p + \ell_i/2$), and $\tau_E^{bulk} \simeq 7\,\mathrm{ms}$, which are to be compared with $\tau_E^{bulk} = \tau_E^{tot} \simeq 5\,\mathrm{ms}$ for an identical ohmic discharge. The value of τ_E^{bulk} is more uncertain than τ_E^{tot} because of the large uncertainty in the determination of P_d noted earlier.

3. SCALING OF ENERGY CONFINEMENT TIME IN LHCD PLASMAS

In this section we discuss the scaling of the global energy confinement time with various plasma parameters. In particular the confinement times obtained in LHCD plasmas are compared with those obtained in OH plasmas under identical conditions (a comparison of LHCD and OH plasmas is shown in Fig. 1). Furthermore, the LHCD confinement time scaling can also be compared with those obtained

in neutral beam heated plasmas. One representative scaling law derived for neutral beam dominated ($P_{AUX}/P_{OH} > 2$) L-mode plasmas is the Kaye-Goldston scaling law[14]. When applied to Alcator C, it is given by

$$\tau_E^{K\text{-}G}(\text{ms}) = 64.0\, I_p^{1.24} P_{tot}^{-0.58} \overline{n}_e^{0.26} B_T^{-0.09},$$

where I_p is in MA, P_{tot} is in MW, $\overline{n}_e$ is in $10^{14}\,\text{cm}^{-3}$, and B_T is in Tesla. The LHCD plasmas are particularly noteworthy in that they are maintained purely by auxiliary power so that $P_{AUX}/P_{OH} = \infty$. A comparison with such a scaling law is only a first step towards characterizing the confinement properties of the LHCD plasmas in relation to better documented neutral beam heated plasmas. In reality, a quantitative determination of $\chi_e(r)$, the electron thermal diffusivity profile, would be needed to determine electron transport in LHCD plasmas. However, such a determination was not performed in the present experiment because the rf power deposition profile is not known experimentally.

In Fig. 8 are shown the energies stored in bulk electrons and ions for both LHCD and OH plasmas as functions of density at constant B_T and I_p. For the LHCD plasmas, note that P_{rf} must also be varied in order to maintain a steady state current, as indicated on the top axis. (The scaling of the confinement time with power cannot be separated from that with density in LHCD experiments.) While the bulk stored energy for the LHCD case is nearly the same as for the OH case at lower densities, it becomes larger than the OH case at higher densities, although the difference in the stored energies are smaller than the difference in the total input powers. (Note that $P_{OH} \simeq 200\,\text{kW}$ is nearly constant at all densities.) The variations of the confinement times for this density scan, obtained following the same procedure as outlined in Sec. 2, are shown in Fig. 9. The difference between the solid circles ($\tau_E^{tot} \equiv W^{tot}/P_{tot}$) and the solid triangles ($\tau_E^{l} \equiv W^{bulk}/P_{tot}$) gives the

contribution of the tail stored energy (W^{tail}/P_{tot}). The relative importance of the tail contribution becomes smaller as the density is increased. The largest source of error in the confinement time measurement arises from the determination of W^{tail}, and the uncertainty becomes largest at the lowest densities considered here. The lower limits of the error bars on τ_E^{tot} correspond to the conservative assumption of $\ell_i/2$ being the same for LHCD and OH cases, adopted in Ref. [5]. We see that τ_E^{tot} for LHCD plasmas decreases gradually with $\overline{n}_e$ (or P_{rf}), whereas it increases linearly with $\overline{n}_e$ for OH plasmas, as expected from neo-Alcator scaling[15] obtained in electron conduction dominated OH plasmas. On the other hand $\tau_E' \equiv W^{bulk}/P_{tot}$, which gives a lower limit on $\tau_E^{bulk} \equiv W^{bulk}/P_d$, is nearly independent of density (or rf power). If the ratio P_d/P_{tot} were a weak function of density, τ_E^{bulk} would scale similarly to τ_E', but would have higher values than τ_E' by a factor P_{tot}/P_d (see Sec. 5 and Table II). The dashed line indicates τ_E calculated for the present experimental parameters using Kaye-Goldston scaling. Whether the good agreement with the experimental τ_E^{tot} is an indication that such a scaling law also holds in LHCD plasmas or is just a coincidence must wait until the LHCD data base is further expanded, including data from other tokamaks.

The most interesting feature of this scaling is a possible indication that the values of τ_E^{tot} obtained at low densities $\overline{n}_e \lesssim 3 \times 10^{13}\,\mathrm{cm}^{-3}$, where plasmas can be maintained with modest rf powers, may exceed the ohmic confinement time. Unfortunately, the uncertainty in evaluating τ_E^{tot} becomes large in this density regime because the fraction of energy stored in the electron tail becomes larger as the density is decreased. The value of $\tau_E' \equiv W^{bulk}/P_{tot}$, with the tail stored energy excluded, also approaches the ohmic value at these densities because P_{tot} approaches the ohmic value and the values of W^{bulk} are similar for the two cases (see Fig. 8).

The radiated power loss did not play an important role in the energy balance at

densities $\overline{n}_e \gtrsim 4 \times 10^{13}\,\mathrm{cm}^{-3}$, and cannot be responsible for the deterioration of τ_E^{tot} at high densities and high rf powers[5]. The spectroscopically determined radiated power due to molybdenum line emission (the dominant impurity species for radiation losses in these plasmas), and Z_{eff} determined from visible Bremsstrahlung, are shown as functions of density in Fig. 10. The absolute value of the radiated power due to molybdenum is uncertain by a factor of two. The bolometrically determined total radiated power behaves similarly, but the absolute calibration is presently more uncertain than the spectroscopic measurements. The rf power needed to maintain a steady state plasma current is also shown in the same figure. Since the fractional radiated power P_{rad}/P_{rf} decreases at least like $1/\overline{n}_e$, the deteriorated global energy confinement time in the LHCD case compared to the OH case cannot be explained by radiation losses.

The scaling of τ_E^{tot} with I_p, corresponding to the case of Fig. 5, is shown in Fig. 11. As with the density scaling experiment, P_{rf} must be varied approximately linearly with I_p to maintain the steady state current. Both the ohmic confinement time and the quantity $\tau_E' \equiv W^{bulk}/P_{tot}$ for the LHCD plasma exhibit a weakly decreasing trend with plasma current. On the other hand, $\tau_E^{tot} \equiv W^{tot}/P_{tot}$, with the electron tail energy included, has an increasing trend, although data are also consistent with a scaling independent of plasma current, because of large uncertainties in the determination of the tail energy using the present method. A more direct measurement of either the tail energy or the current density profile is needed in order to reduce these uncertainties.

The scaling of τ_E^{tot} with the toroidal magnetic field was also studied in the range B_T = 7–11 T. Because the current drive efficiency increases with toroidal field[4], the rf power was lowered as B_T was raised. The ohmic power remained constant with B_T. Both τ_E' and τ_E^{tot} for the LHCD plasmas increased by nearly

50% when the toroidal field was increased from $B_T = 6.9\,\mathrm{T}$ to $10.4\,\mathrm{T}$ (with a corresponding decrease in P_{tot} from 380 to 620kW), while the ohmic confinement time was nearly independent of B_T, as shown in Fig. 12. The global energy confinement time, τ_E^{tot}, of the LHCD plasmas were again comparable in magnitude to ohmic values. Because the profile data for this scan were not as complete as those for the density and current scans, we have assumed that $\ell_i/2$ for the LHCD and OH cases were the same in order to obtain W^{tail} for the LHCD plasmas, which results in an underestimate of the tail stored energy. If we assume that there is no explicit dependence of τ_E^{tot} on B_T, the toroidal field scan for the LHCD case is equivalent to a power scan at fixed $\overline{n}_e$ and I_p, indicating that the deterioration of τ_E^{tot} relative to ohmic values observed at higher densities may really be a deterioration with power alone rather than with density.

4. THE EFFECT OF INDUCTIVE ELECTRIC FIELD

In order to study the transition from purely OH to purely LHCD discharges, and to investigate a possible existence of an optimum regime in combined OH-LHCD plasmas, we have varied P_{rf}, keeping other parameters constant at $B_T = 8\,\mathrm{T}$, $I_p = 200\,\mathrm{kA}$, and $\overline{n}_e = 4 \times 10^{13}\,\mathrm{cm}^{-3}$. The plasma current was feedback controlled so that P_{OH} varied accordingly ($P_{rf}/P_{OH} = 0 \rightarrow \infty$). An OH shot, a fully rf-driven LHCD shot, and a combined OH-LHCD shot are shown in Fig. 13. As shown in Fig. 14 we find that with the application of even a small amount of P_{rf}, W^{tail} increases significantly because of combined effects of rf velocity space diffusion and acceleration due to the inductive electric field. The internal inductance $\ell_i/2$ was again assumed to be unchanged by the application of rf power. On the other hand, for $P_{rf} \lesssim 150\,\mathrm{kW}$ corresponding to rf powers less than approximately half of the original ohmic power, the total input power P_{tot} actually drops because the decrease

in the loop voltage more than compensates for the added amount of P_{rf} as shown in Fig. 15. The result is an increased τ_E^{tot} in these combined OH-LHCD plasmas, as shown in Fig. 16. However, W^{tail} does not increase appreciably as P_{rf} is increased further, and τ_E^{tot} drops to a value comparable to the ohmic value when all the current is replaced by the rf current ($P_{rf}/P_{OH} = \infty$). If the current profile did not stay constant but broadened with increasing rf power, the tail energy W^{tail} would be underestimated at high rf powers. The quantity $\tau_E' \equiv W^{bulk}/P_{tot}$, which represents a lower limit on the bulk energy confinement time $\tau_E^{bulk} \equiv W^{bulk}/P_d$, is comparable to the ohmic case when P_{tot} is comparable to that for the purely ohmic case, but it deteriorates with increasing P_{tot}. An improved τ_E' over the ohmic value has been reported from the Petula–B tokamak, although the maximum in τ_E' was obtained when T_e took the minimum value[16]. In the present experiments, the bulk electron stored energy stays roughly constant at $W_e^{bulk} \simeq 1.1\,\mathrm{kJ}$ for the entire range of P_{rf}/P_{OH} and no significant temperature drops were observed. In larger machines with better electron tail confinement, additional heating of the bulk plasma and an improved τ_E' might be expected in this regime.

5. NUMERICAL MODELING

In order to interpret the experimental results presented in Sec. 3, particularly the deterioration of the global energy confinement time τ_E^{tot} at higher densities (and powers), we have used a ray tracing-Fokker Planck-transport code developed by Bonoli and Englade[17] to model energy confinement properties in these purely LHCD plasmas. We have considered some possible causes of the degraded confinement time, such as an enhanced thermal diffusivity of the bulk plasma over the ohmic value, poor rf absorption efficiency, broader (or even hollow) rf power deposition profiles relative to ohmic power deposition profiles, and poor electron tail

confinement.

The wave absorption and the modification of the distribution function are treated self-consistently in the code. The effect of enhanced perpendicular temperature of the tail is modeled using the formalism of Fuchs, et al.[18] A direct electron tail loss mechanism due to radial diffusion was included and was modeled with a phenomenological energy dependent confinement time[19] of the form $\tau_l = \tau_0 \gamma^3$, where τ_0 has a value comparable to the bulk electron energy confinement time τ_{Ee} in LHCD plasmas. This form of the electron tail confinement time reflects the notion that higher energy electrons experience less radial transport[20]. The radial diffusion of the rf current, corresponding to the diffusion of high energy electrons, was modeled by an anomalous current diffusion coefficient (compared to classical resistive diffusion), whose magnitude was approximately 0.2 times the bulk thermal diffusivity. The magnitude of the current diffusion coefficient is determined self-consistently with the electron tail loss model discussed above, and corresponds to an energy average of the velocity dependent diffusivity[19]. This model reproduced centrally peaked current density profiles experimentally indicated by the peaked plasma hard X-ray profiles, and the time scale (typically 20ms) for the surface loop voltage drop. Such a diffusion may be driven by the tendency of the plasma to assume a self-consistent current density profile[21]. Slowing down of these high energy electrons would then produce a centrally peaked bulk heating profile. The profile of the collisional slowing down power was diffused accordingly, and the resulting profile was used as the bulk electron source term in the transport code. The electron thermal transport was modeled with the bulk electron thermal diffusivity proposed by Tang[22]. The electron thermal diffusivity in LHCD plasmas was taken to have the same radial profile as that in OH plasmas, with a constant enhancement factor across the whole profile, so that $\chi_e^{LHCD}(r) = M_e \chi_e^{OH}(r)$ where M_e is a constant

multiplier. The ion diffusivity $\chi_i(r)$ was modeled as a constant multiplier times the neo-classical diffusivity[23,24], and the same multiplier was used for LHCD case and the OH case.

The tail confinement time parameter τ_0 (and therefore, the rf current diffusivity) is determined by the requirement to match the experimental current drive efficiency, and was found to be represented well by a constant value of $\tau_0 = 3.25\,\mathrm{ms}$ at all densities. The minimum amount of power which must be supplied in order to maintain a given amount of steady state current is given by the power dissipated collisionally on the bulk electrons, P_d. If the rf absorption efficiency were not perfect ($\eta_{abs} \equiv P_{abs}/P_{rf} < 1$), or in the presence of finite radial tail losses ($P_l \equiv W^{tail}/\tau_E^{tail} > 0$), the current drive efficiency $\eta_{CD} \equiv \overline{n}_e I_p R/P_{rf}$ would become lower than the ideal case because more input rf power P_{rf} is required (see Fig. 2). The possibilities that the degradation of rf absorption efficiency or an increased fraction of direct electron tail loss are responsible for the confinement deterioration at higher densities must be ruled out because of the restriction on η_{CD}, which has been observed experimentally to be roughly independent of density. The only free parameter remaining is the electron thermal diffusivity multiplier M_e, which represents the degree of degradation of the bulk electron energy confinement relative to ohmic plasmas. The value of M_e was adjusted to reproduce the experimental electron temperature profile.

The rf power deposition profiles $P_e(r)$ (power absorbed by electron Landau damping and collisional damping) predicted by the code at different densities are shown in Fig. 17. Direct collisional damping of the incident waves is significant only near the plasma edge and accounts for less than 20% of the total input power even at the highest density $\overline{n}_e = 7 \times 10^{13}\,\mathrm{cm}^{-3}$. The deposition profiles are fairly similar for the three densities shown, with a slightly more central deposition at the

lower densities, but by itself not enough to account for the observed deterioration of energy confinement. In the presence of spatial diffusion, the bulk electron heating profile becomes more centrally peaked. Within the limitations imposed by the code model, it can be concluded that the confinement degradation cannot be explained by a change in the power deposition profile, but can be attributed to the increased enhancement factor M_e over the ohmic diffusivity as the density and the input rf power are increased.

The results of the numerical simulations are summarized in Table II. Here, P_{abs} is the power absorbed by electron Landau damping, P_d is the power dissipated on bulk electrons by collisional slowing down, and P_l is the direct power loss from the electron tail due to radial transport (see the diagram shown in Fig. 2). The power not absorbed by electron Landau damping, $P_{tot} - P_{abs}$, was absorbed near the plasma edge by collisional damping. The confinement times are defined as $\tau_E^{tot} \equiv W^{tot}/P_{tot}$ and $\tau_E^{bulk} \equiv W^{bulk}/P_d$. We see that while the low density ($\overline{n}_e = 3 \times 10^{13}\,\mathrm{cm}^{-3}$) plasma can be modeled satisfactorily with diffusivities similar to those of ohmic plasmas, the diffusivity had to be enhanced by a factor of approximately 2 over the ohmic value at higher densities. In contrast to the ohmic diffusivity which is inversely proportional to the density, the diffusivity in LHCD plasmas is nearly independent of density if no explicit dependence on input power is assumed. Alternatively, a direct dependence of χ_e on the heating power[25] may be cancelling the density dependence, although such a direct scaling with power cannot be confirmed experimentally in LHCD plasmas.

6. CONCLUSIONS

Energy confinement properties of purely rf maintained LHCD plasmas and combined OH-LHCD plasmas have been studied. In purely LHCD plasmas, both the

magnitude and the scaling of τ_E^{tot} with $\overline{n}_e$ (and simultaneously with P_{tot}) appear to be similar to those predicted by Kaye-Goldston scaling. The scalings with I_p and B_T are more uncertain because of limited ranges investigated. At lower densities, $\overline{n}_e \lesssim 3 \times 10^{13}\,\mathrm{cm}^{-3}$, where a LHCD plasma can be maintained with modest rf powers, τ_E^{tot} was found to be comparable to, or even exceed the ohmic confinement times. However, at higher densities where substantially more rf power (compared to the ohmic power) is needed to maintain a purely rf-driven LHCD plasma, a deterioration of τ_E^{tot} relative to the ohmic confinement time is observed. This deterioration is likely to be associated with increasing power rather than with the density itself.

At low densities in LHCD plasmas, W^{tail} can be a significant fraction of W^{tot}. Furthermore, our measurements and numerical modeling suggest that a significant fraction of the absorbed power is lost directly from the high energy electron tail before thermalizing by collisions on the bulk plasma, especially at low densities. In future large scale experiments in which the energy slowing down time is short compared to the tail electron energy confinement time, this tail loss is expected to become unimportant, which may result in an improvement in bulk plasma heating efficiency.

Results of code modeling indicate that the observed deterioration of τ_E^{tot} at high densities (and high rf powers) is caused by an enhanced electron thermal diffusivity over the ohmic value, rather than mechanisms such as a reduced absorption efficiency, an increased electron tail loss, or an off-central deposition profile.

In combined OH-LHCD plasmas, τ_E^{tot} exceeding the ohmic value could be obtained even at higher densities and higher currents ($\overline{n}_e = 4 \times 10^{13}\,\mathrm{cm}^{-3}$ and $I_p = 200\,\mathrm{kA}$). The global energy confinement time, τ_E^{tot} was maximized when the applied rf power was comparable to the residual ohmic power, which was approximately half of the original ohmic input power. With better tail confinement in larger machines

additional heating of the bulk plasma in this regime may be expected. Because this improved τ_E^{tot} regime is obtained when the plasma current is not completely replaced by the rf driven current, the rf power requirements are reduced. Such a regime is expected to extend up to even higher densities (up to the current drive density limit[26]), and may prove to be an attractive way to enhance energy confinement. Recent sawtooth stabilization experiments[27,28] were carried out in this mode of operation. Energy confinement in combined experiments using lower hybrid and other forms of auxiliary heating methods remains a subject of future study.

ACKNOWLEDGMENTS

We would like to thank the entire Alcator group for their contributions, especially Mr. D. Griffin for his engineering support, and Dr. S. Wolfe for useful discussions. This work was supported by U.S. Department of Energy Contract No. DE–AC02–78ET51013.

REFERENCES

[1] KAYE, S. M., Phys. Fluids **28** (1985) 2327.

[2] See for example, the following review papers: PORKOLAB, M., in Course and Workshop on Application of RF Waves on Tokamaks, Vol. 1, Int. School of Plasma Physics, Milano (1985) 288; WILSON, R., ibid., 146; PRATER, R., ibid., 354.

[3] JACQUINOT, J., ANDERSON, R. J., ARBEZ, J., BARTLETT, D., BEAUMONT, B., et al., Plasma Phys. and Controlled Fusion 28A (1986) 1.

[4] PORKOLAB, M., SCHUSS, J. J., LLOYD, B., TAKASE, Y., TEXTER, S., et al., Phys. Rev. Lett. **53** (1984) 450.

[5] KNOWLTON, S., PORKOLAB, M., TAKASE, Y., TEXTER, S., BONOLI, P., et al., Energy Confinement of Lower Hybrid Current Driven Tokamak Plasmas, MIT Plasma Fusion Center Report PFC/JA–86–4 (1986); submitted to Phys. Rev. Lett.

[6] TEXTER, S., BONOLI, P., KNOWLTON, S., PORKOLAB, M., TAKASE, Y., Energy Confinement of the High Energy Tail Electrons During Lower Hybrid Current Drive on the Alcator C Tokamak, MIT Plasma Fusion Center Report PFC/JA–86–10; submitted to Nucl. Fusion.

[7] BONOLI, P., ENGLADE, R., Simulation Model for Lower Hybrid Current Drive, MIT Plasma Fusion Center Report PFC/JA–86–5 (1986); accepted for publication in Phys. Fluids.

[8] PORKOLAB, M., LLOYD, B., TAKASE, Y., BONOLI, P., FIORE, C, et al., Phys. Rev. Lett. **53** (1984) 1229.

[9] SHAFRANOV, V. D., in Review of Plasma Physics, Vol. 2, ed. by M. A. Lentovich, Consultants Bureau, New York (1966) 103.

[10] MONDELLI, A., OTT, E., Phys. Fluids **17** (1974) 1017.

[11] McCORMICK, K., SÖLDNER, F. X., LEUTERER, F., MURMANN, H., ECKHARTT, D., et al., Influence of the Lower Hybrid Wave Spectrum on the Current Distribution in ASDEX, paper presented at 13th Eur. Conf. on Controlled Fusion and Plasma Physics, Schliersee, West Germany, April 1986 (proc. to be published).

[12] TEXTER, S., KNOWLTON, S., PORKOLAB, M., TAKASE, Y., High Energy X-ray Measurements During Lower Hybrid Current Drive on the Alcator C Tokamak, MIT Plasma Fusion Center Report PFC/JA–86–11; submitted to Nucl. Fusion.

[13] STEVENS, J., VON GOELER, S., BERNABEI, S., BITTER, M., CHU, T. K., et al., Nucl. Fusion **25** (1985) 1529.

[14] KAYE, S. M., GOLDSTON, R. J., Nucl. Fusion **25** (1985) 65.

[15] BLACKWELL, B., FIORE, C. L., GANDY, R., GONDHALEKAR, A., GRANETZ, R. S., et al., in Plasma Physics and Controlled Nuclear Fusion Research, (Proc. 9th Int. Conf., Baltimore, 1982) Vol. 2, IAEA, Vienna (1983) 27.

[16] GORMEZANO, C., BLANC, P., BOTTOLLIER, H., BRIAND, P., BRIFFOD, G., et al., in Radiofrequency Plasma Heating, (Proc. 6th Top. Conf., Callaway Gardens, GA, 1985) AIP, New York (1985) 111.

[17] BONOLI, P., ENGLADE, R., PORKOLAB, M., in Heating in Toroidal Plasmas (Proc. 4th Int. Symp., Rome, 1984) Vol. 2, Int. School of Plasma Physics, Varenna (1984) 1311.

[18] FUCHS, V., CAIRNS, R. A., SHOUCRI, M. M., HIZANIDIS, K., BERS, A., Phys. Fluids **28** (1985) 3619.

[19] ENGLADE, R., BONOLI, P., in Radiofrequency Plasma Heating, (Proc. 6th Top. Conf., Callaway Gardens, GA, 1985) AIP, New York (1985) 151.

[20] MYNICK, H., STRACHAN, J., Phys. Fluids **24** (1981) 695.

[21] COPPI, B., Comments on Plasma Phys. and Controlled Fusion **5** (1980) 261.

[22] TANG, W. M., Microinstability-Based Model for Anomalous Thermal Confinement in Tokamaks, Princeton Plasma Physics Laboratory Report PPPL–2311 (1986); to be published.

[23] CHANG, C. S., HINTON, F. L., Phys. Fluids **25** (1982) 1493.

[24] HINTON, F. L., HAZELTINE, R. D., Rev. Mod. Phys. **48** (1976) 239.

[25] WAGNER, F., GRUBER, O., LACKNER, K., MURMANN, H. D., SPETH, E., et al., Phys. Rev. Lett. **56** (1986) 2187.

[26] PORKOLAB, M., in Wave Heating and Current Drive in Plasmas, ed. by V. L. Granastein and P. L. Colestock, Gordon and Breach, New York (1985) 260.

[27] PORKOLAB, M., KNOWLTON, S., TAKASE, Y., TEXTER, S., BONOLI, P., et al., Bull. Am. Phys. Soc. **30** (1985) 1493; also paper presented at 13th Eur. Conf. on Controlled Fusion and Plasma Physics, Schliersee, W. Germany, April 1986 (proc. to be published).

[28] CHU, T. K., BELL, R., BERNABEI, S., CAVALLO, A., HOOKE, W., et al., Radiofrequency Plasma Heating (Proc. 6th Top. Conf., Callaway Gardens, GA, 1985) AIP, New York (1985) 131.

TABLE I. A summary of power balance for a typical LHCD plasma and a corresponding OH plasma. Hydrogen, $B = 8\,\mathrm{T}$, $I_p = 140\,\mathrm{kA}$, $\overline{n}_e = 3 \times 10^{13}\,\mathrm{cm}^{-3}$. Symbols are defined in the text. The tail energy W^{tail} and the collisionally dissipated power P_d were obtained using the tail distribution function f_e^{tail} inferred from plasma hard X-ray measurements.

	P_{tot}	P_d	W^{bulk}	W^{tail}	W^{tot}	τ_E^{bulk}	τ_E^{tot}
LHCD	300kW	150kW	1.0kJ	1.4kJ	2.4kJ	7ms	8ms
OH	200kW	—	1.0kJ	—	1.0kJ	5ms	5ms

TABLE II. A summary of the results of numerical modeling for LHCD and OH plasmas at three different densities. Hydrogen, $B = 8\,\mathrm{T}$, $I_p = 140\,\mathrm{kA}$. Symbols are defined in the text.

	$\overline{n}_e$ ($10^{13}\,\mathrm{cm}^{-3}$)	P_{tot} (kW)	P_{abs} (kW)	P_d (kW)	P_l (kW)	W^{bulk} (kJ)	W^{tail} (kJ)	τ_E^{bulk} (ms)	τ_E^{tot} (ms)	M_e
LHCD	3	320	302	209	93	1.20	1.01	5.7	6.9	1.0
	5.5	650	590	472	117	2.10	1.11	4.4	4.9	2.0
	7	950	779	652	127	3.00	0.99	4.6	4.2	2.3
OH	3	190	—	—	—	1.10	—	5.8	5.8	—
	5.5	210	—	—	—	2.00	—	9.5	9.5	—
	7	230	—	—	—	2.40	—	10.4	10.4	—

FIGURE CAPTIONS

FIG. 1. A typical LHCD shot (solid line) and an OH comparison shot (dashed line). Hydrogen, $B = 8\,\mathrm{T}$, $I_p = 140\,\mathrm{kA}$, $\overline{n}_e = 4 \times 10^{13}\,\mathrm{cm}^{-3}$, $P_{rf} = 500\,\mathrm{kW}$ (LHCD), $P_{OH} = 200\,\mathrm{kW}$ (OH).

FIG. 2. A schematic diagram of power balance during LHCD. The plasma, represented by the rectangle, is divided into the electron tail and the bulk plasma (electrons and ions).

FIG. 3. Time evolutions of the central electron temperature (Thomson scattering) obtained on a shot-by-shot basis for LHCD (solid circles) and OH comparison (open triangles) shots shown in Fig. 1. Also shown are plasma current waveforms for LHCD (solid line) and OH (dashed line) shots.

FIG. 4. Electron temperature profiles for LHCD (solid circles) and OH (open triangles) plasmas, as measured by Thomson scattering. The curves represent gaussian fits to the data points. Hydrogen, $B = 8\,\mathrm{T}$, $I_p = 110\,\mathrm{kA}$, $\overline{n}_e = 3.5 \times 10^{13}\,\mathrm{cm}^{-3}$. The limiter radius is $a = 16.5\,\mathrm{cm}$.

FIG. 5. $\beta_p + \ell_i/2$ determined from the equilibrium field measurement as a function of plasma current for LHCD (solid circles) and OH (open circles) plasmas. Also shown are β_p^{bulk} determined from the profile analysis for LHCD (solid triangles) and OH (open triangles) plasmas. The solid squares represent estimated values of $\beta_p^{bulk} + \ell_i/2$ for LHCD plasmas with $\ell_i/2$ determined from the electron temperature profiles. The error bars indicate uncertainty in relating the temperature profile to the current density profile (see text). Hydrogen plasma, $B = 8\,\mathrm{T}$, $\overline{n}_e = 4 \times 10^{13}\,\mathrm{cm}^{-3}$.

FIG. 6. (a) The central electron temperature and (b) the gaussian profile width as functions of plasma current. These plasmas are not sawtoothing ($q \gtrsim 8$). Same parameters as Fig. 5.

FIG. 7. The plasma hard X-ray gaussian profile width at different energies as functions of current. Same parameters as Fig. 5.

FIG. 8. The stored energy in the bulk electrons and ions as a function of density for LHCD (solid circles) and OH (open circles) plasmas. The rf power was varied as shown on the top axis in order to maintain a fixed steady state current. Hydrogen plasma, $B = 8\,\mathrm{T}$, $I_p = 140\,\mathrm{kA}$.

FIG. 9. The global energy confinement time $\tau_E^{tot} \equiv W^{tot}/P_{tot}$ as a function of density for both LHCD (solid circles) and OH (open triangles) plasmas. Hydrogen plasma, $B = 8\,\mathrm{T}$, $I_p = 140\,\mathrm{kA}$ (same parameters as Fig. 8). Also shown is $\tau_E' \equiv W^{bulk}/P_{tot}$ for LHCD plasmas (solid triangles). Kaye-Goldston scaling for the the present experimental conditions is shown with the dashed line.

FIG. 10. The spectroscopically determined radiated power due to molybdenum line emission (solid circles) and Z_{eff} (open triangles) as functions of density. The rf power needed to maintain a steady state current (which is equal to the total input power) is also shown (open circles). Same parameters as Fig. 9.

FIG. 11. The energy confinement times as functions of plasma current. Hydrogen plasma, $B = 8\,\mathrm{T}$, $\overline{n}_e = 4 \times 10^{13}\,\mathrm{cm}^{-3}$ (same parameters as Fig. 5). The rf power was varied as shown on the top axis to maintain a steady state current at a fixed density. The dashed line represents Kaye-Goldston scaling.

FIG. 12. The energy confinement times as functions of toroidal field in hydrogen plasmas. The rf power was varied as shown on the top axis to maintain a steady state current at fixed density and current of $\overline{n}_e = 4 \times 10^{13}\,\mathrm{cm}^{-3}$ and $I_p = 150\,\mathrm{kA}$, respectively. The dashed line represents Kaye-Goldston scaling.

FIG. 13. A purely OH shot (dotted line), a purely LHCD shot (solid line), and a combined OH and LHCD shot (dashed line). Hydrogen plasma, $B = 8\,\mathrm{T}$, $I_p = 200\,\mathrm{kA}$, $\overline{n}_e = 4 \times 10^{13}\,\mathrm{cm}^{-3}$.

FIG. 14. The total stored energy as a function of P_{tot} with in combined OH and LHCD plasmas. The ratio P_{rf}/P_{OH} varies from 0 (purely OH, shown by the open triangle) to ∞ (purely LHCD, shown by the open circle). Hydrogen plasma, $B = 8\,\mathrm{T}$, $I_p = 200\,\mathrm{kA}$, $\overline{n}_e = 4 \times 10^{13}\,\mathrm{cm}^{-3}$.

FIG. 15. The variations of the ohmic input power P_{OH} and the total input power P_{tot} as the rf power P_{rf} is varied. Same conditions as Fig. 14. The ohmic primary circuit was feedback controlled to maintain a constant plasma current.

FIG. 16. The confinement times $\tau_E^{tot} \equiv W^{tot}/P_{tot}$ (circles) and $\tau_E' \equiv W^{bulk}/P_{tot}$ (squares) as functions of P_{rf}. The open triangle is purely OH while the open circle and open square are purely LHCD. The arrows indicate the direction of increasing P_{rf}. Same parameters as Fig. 14.

FIG. 17. The rf power deposition profiles predicted by the ray tracing-Fokker Planck-transport code at three different densities.

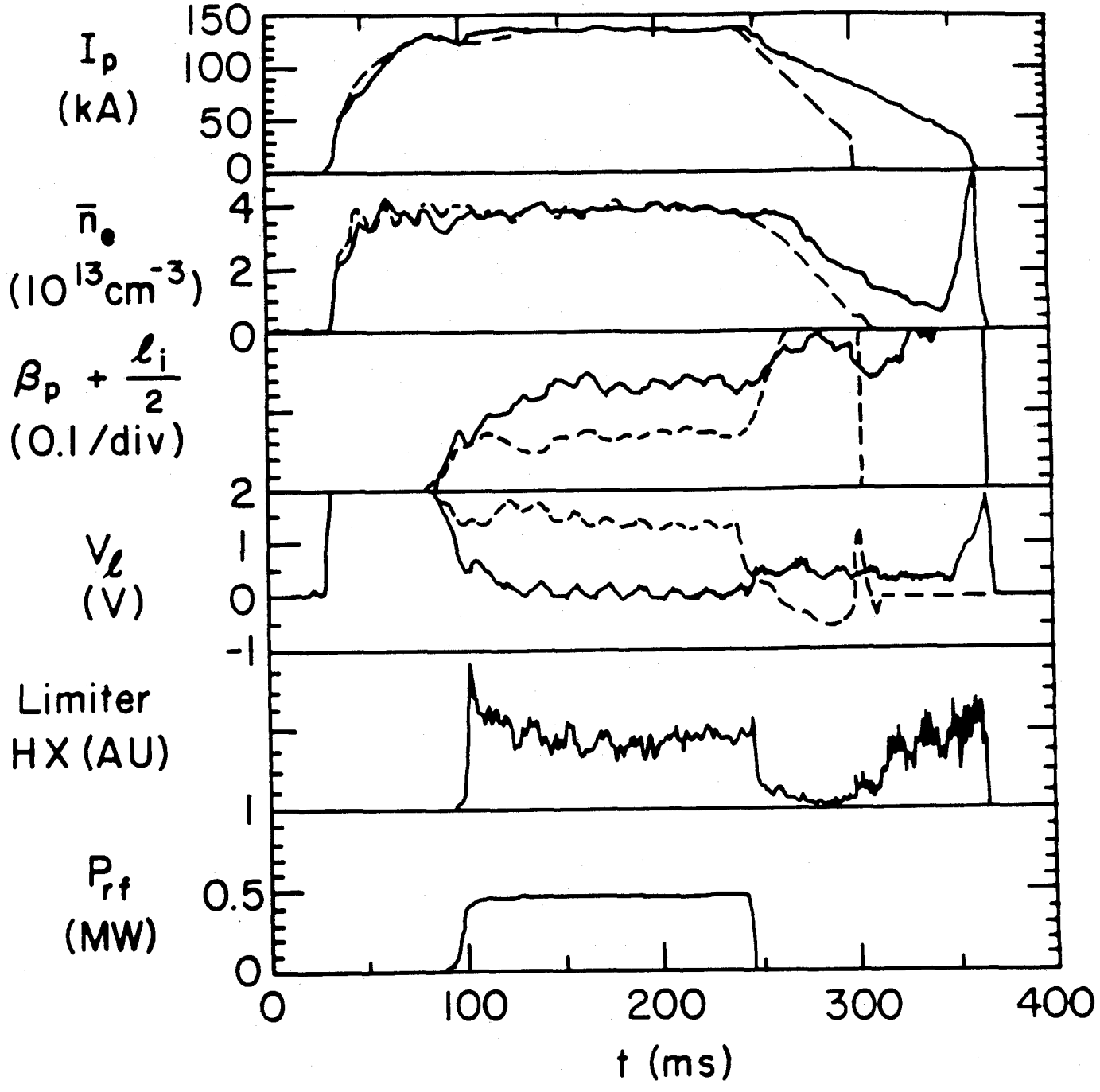
I_p
(kA)
150
100
50
0
$\bar{n}_e$
$(10^{13}cm^{-3})$
4
2
0
$\beta_p + \frac{\ell_i}{2}$
(0.1/div)
2
1
0
-1
V_ℓ
(V)
Limiter
HX (AU)
1
P_{rf}
(MW)
0.5
0
0
100
200
300
400
t (ms)

Fig. 1

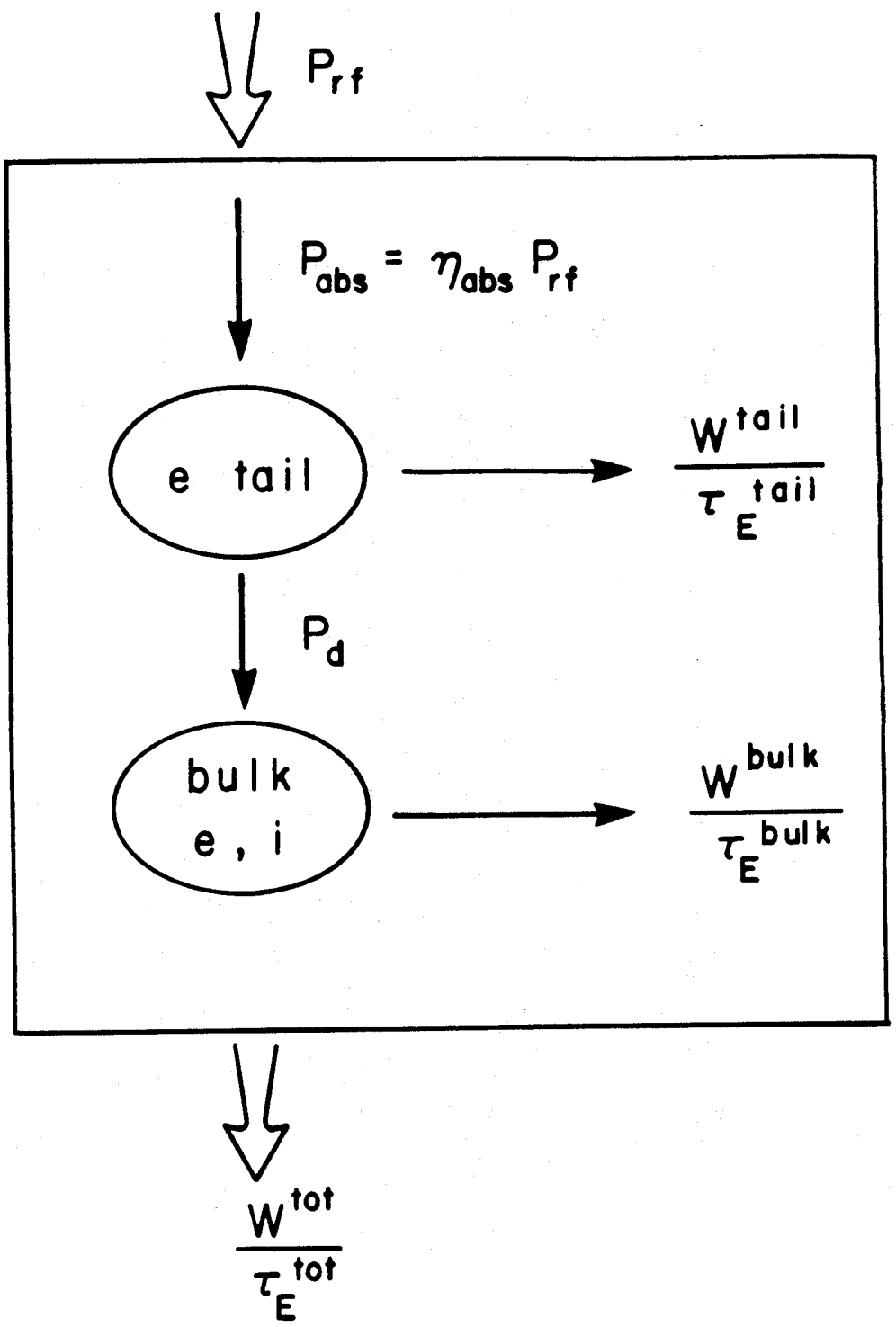
P_{rf}
$P_{abs} = \eta_{abs} P_{rf}$
e tail
$\frac{W^{tail}}{\tau_E^{tail}}$
P_d
bulk
e , i
$\frac{W^{bulk}}{\tau_E^{bulk}}$
$\frac{W^{tot}}{\tau_E^{tot}}$

Fig. 2

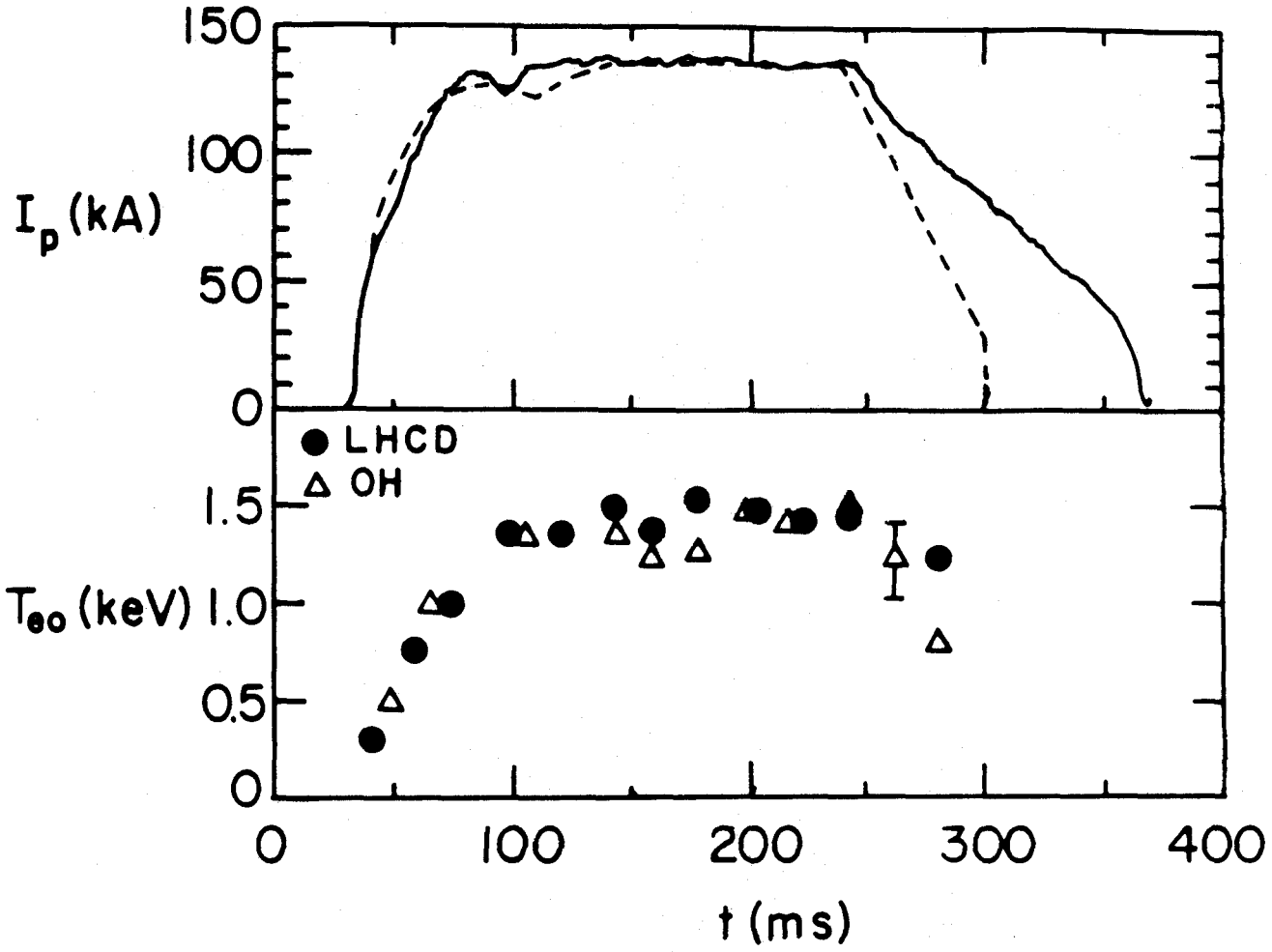

Fig. 3

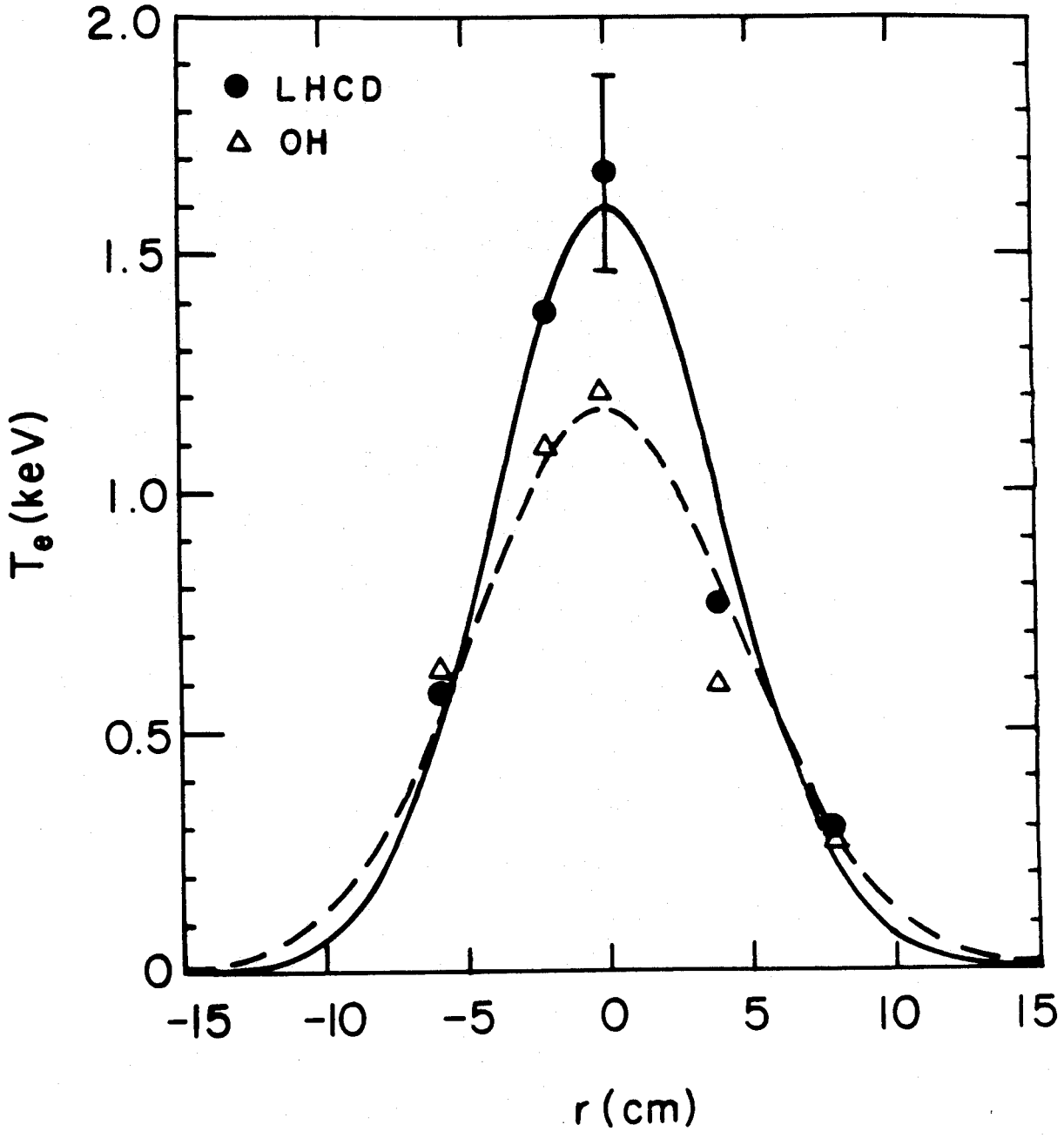

Fig. 4

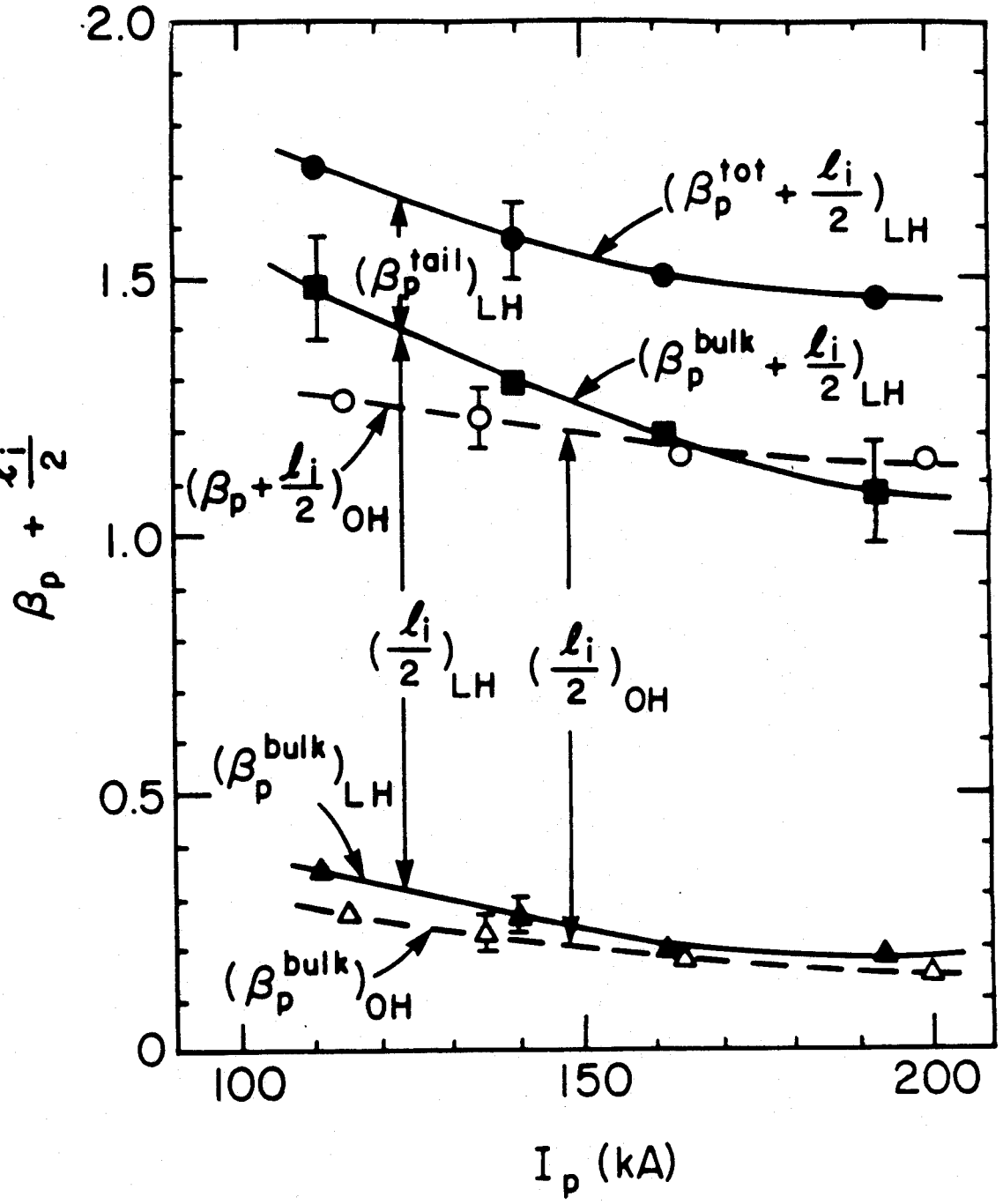
2.0
1.5
1.0
0.5
0
100
150
200
I_p (kA)
$\beta_p + \frac{\ell_i}{2}$
$(\beta_p^{tot} + \frac{\ell_i}{2})_{LH}$
$(\beta_p^{tail})_{LH}$
$(\beta_p^{bulk} + \frac{\ell_i}{2})_{LH}$
$(\beta_p + \frac{\ell_i}{2})_{OH}$
$(\frac{\ell_i}{2})_{LH}$
$(\frac{\ell_i}{2})_{OH}$
$(\beta_p^{bulk})_{LH}$
$(\beta_p^{bulk})_{OH}$

Fig. 5

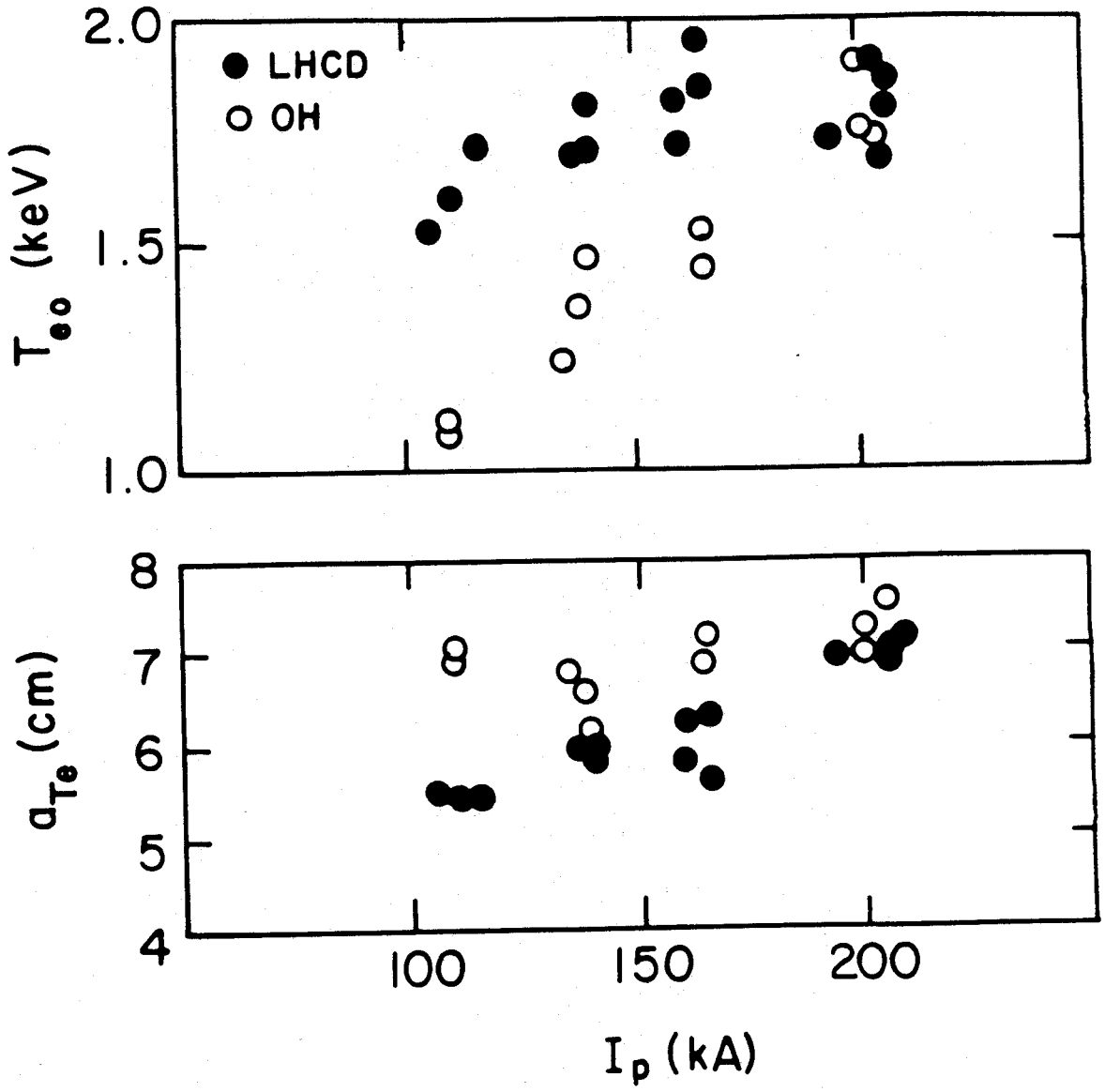

Fig. 6

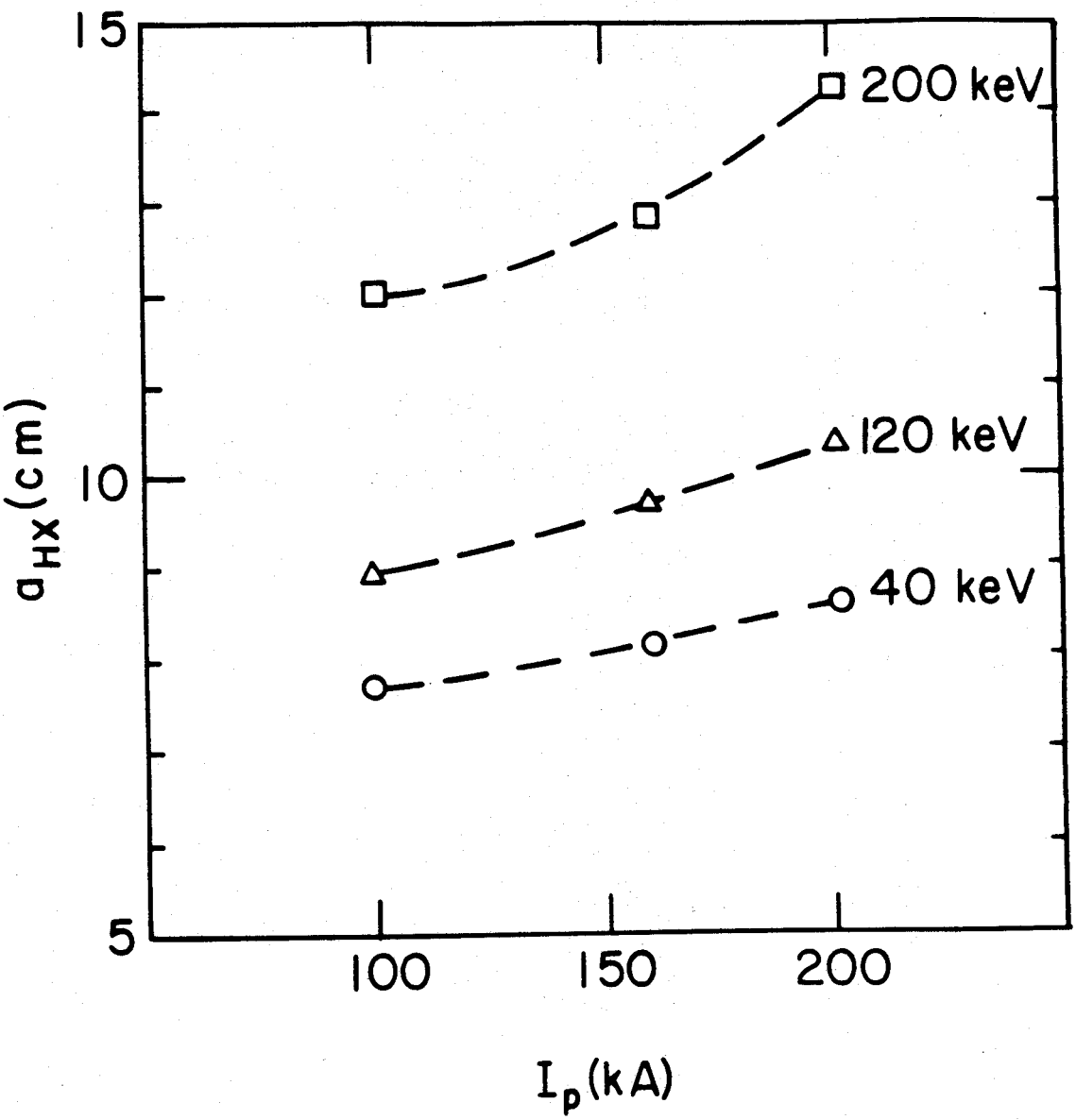

Fig. 7

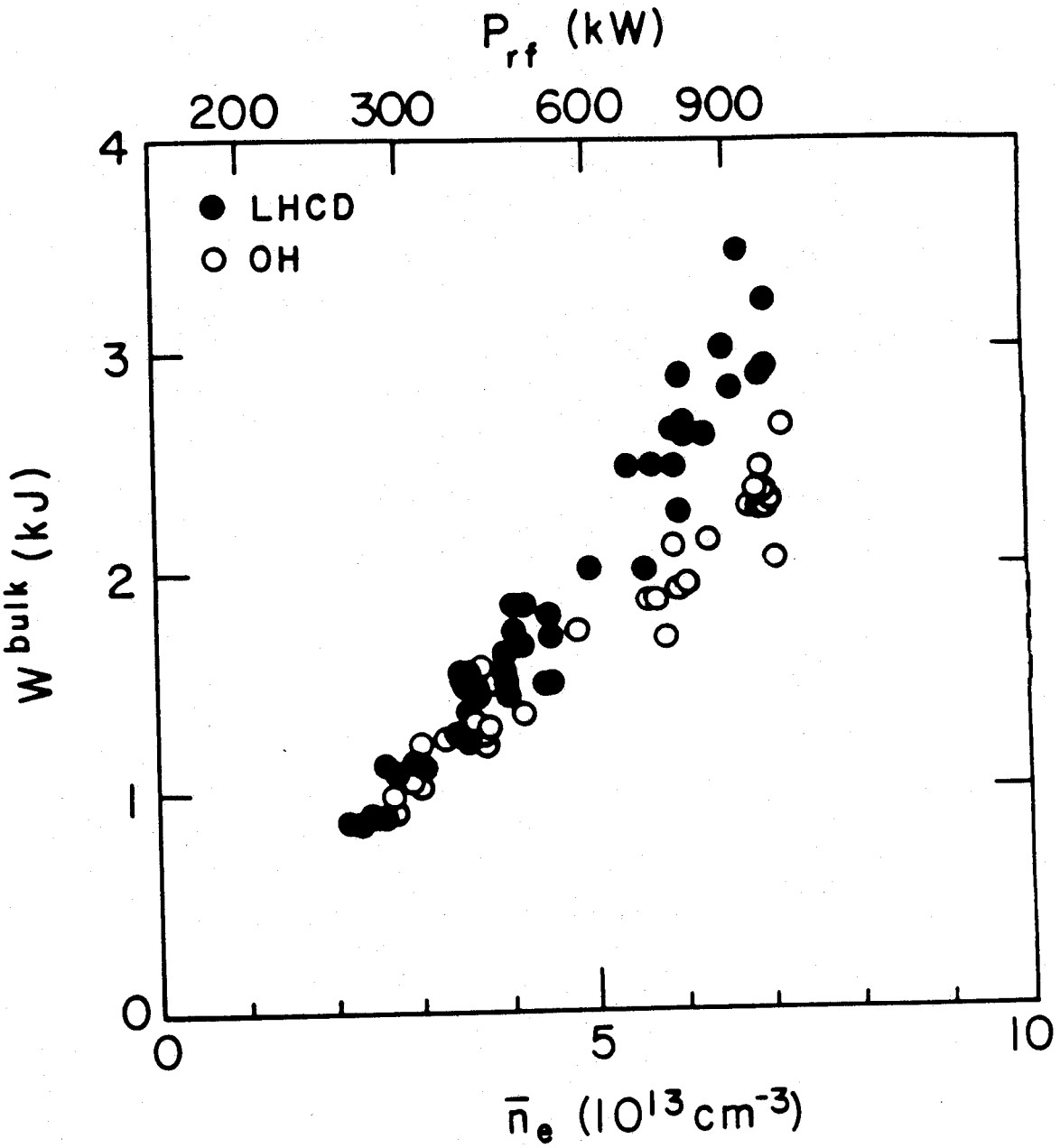

Fig. 8

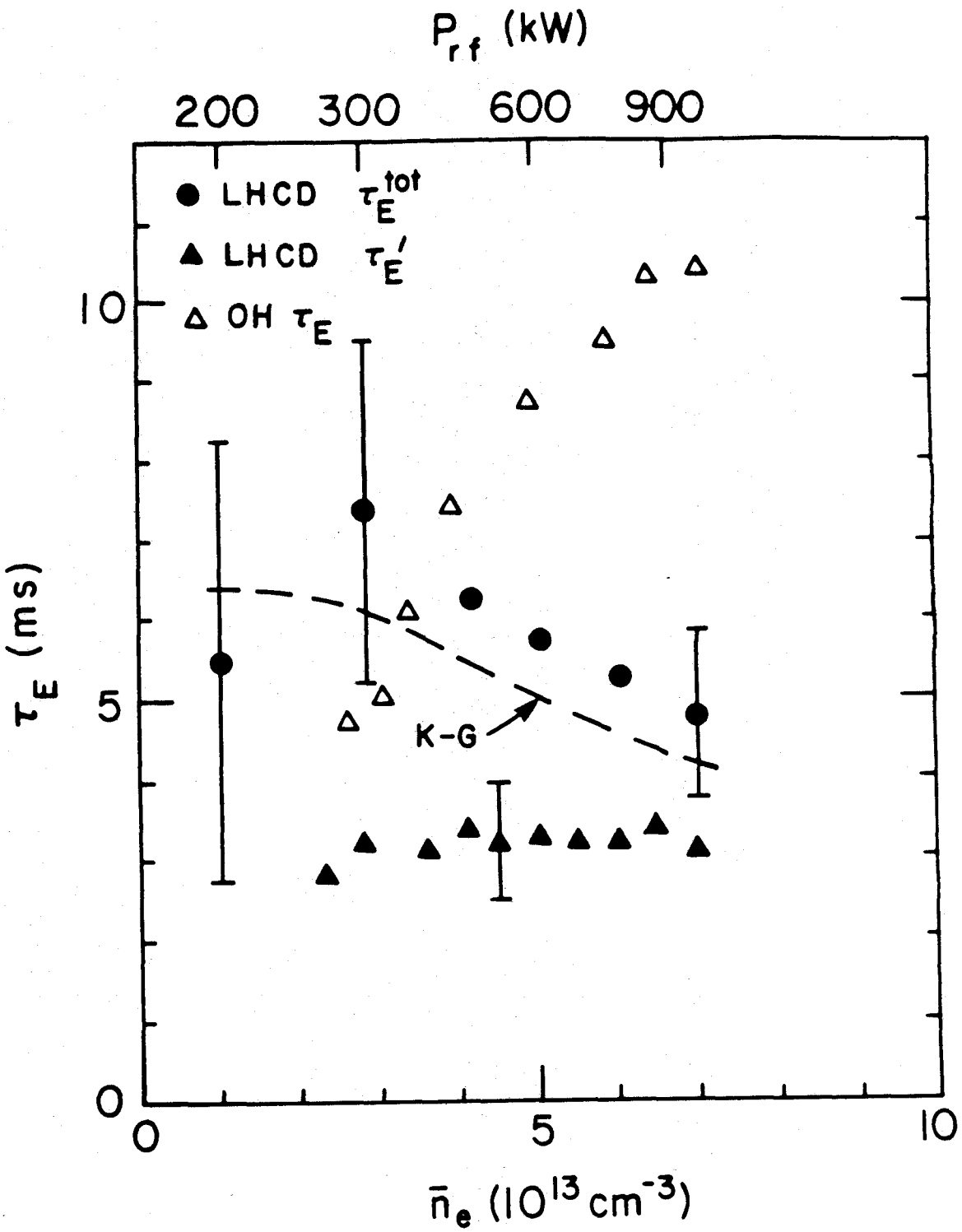
P_{rf} (kW)
200
300
600
900
● LHCD τ_E^{tot}
▲ LHCD τ_E'
△ OH τ_E
10
5
0
τ_E (ms)
K-G
0
5
10
$\bar{n}_e$ (10^{13} cm^{-3})

Fig. 9

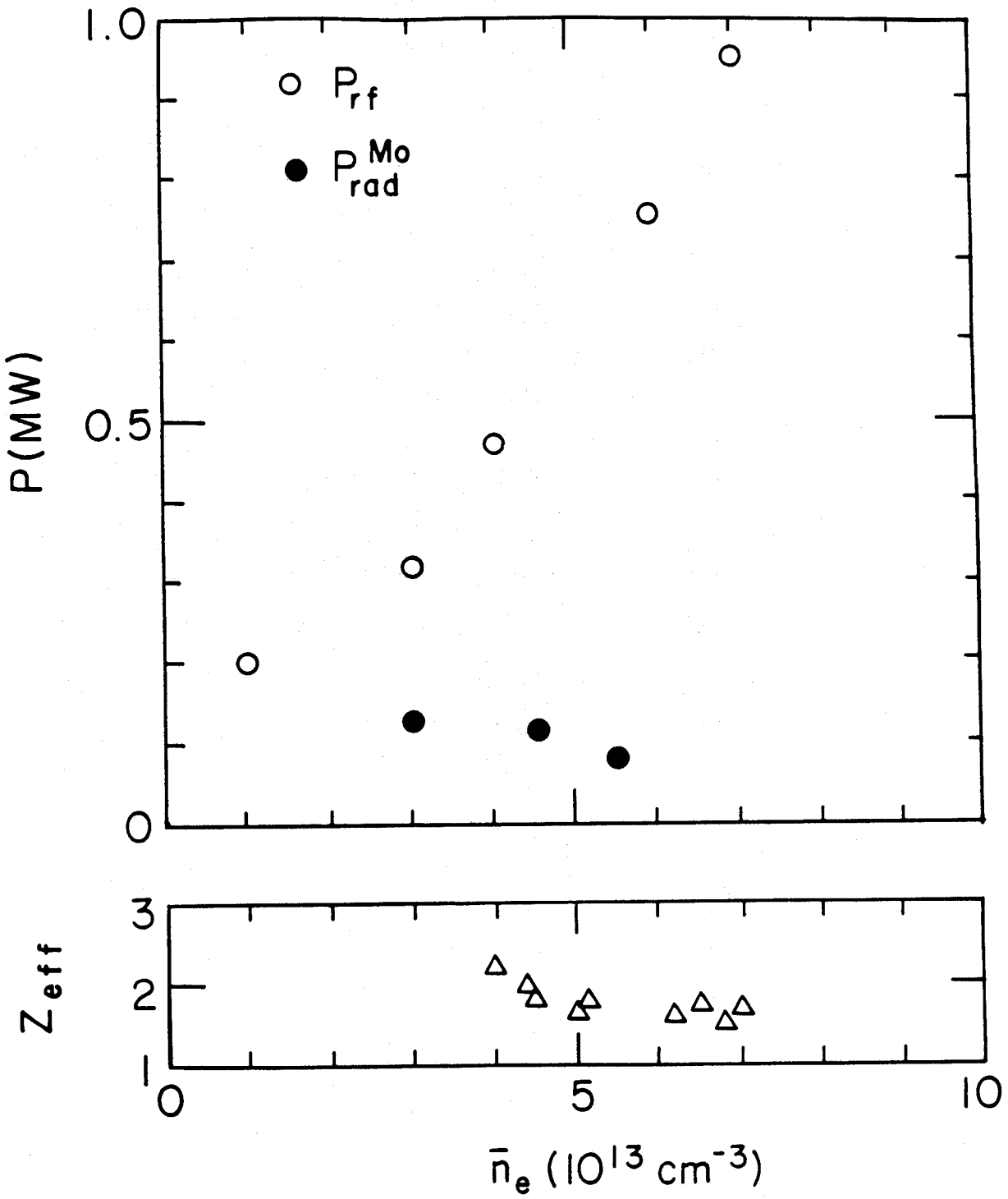

Fig. 10

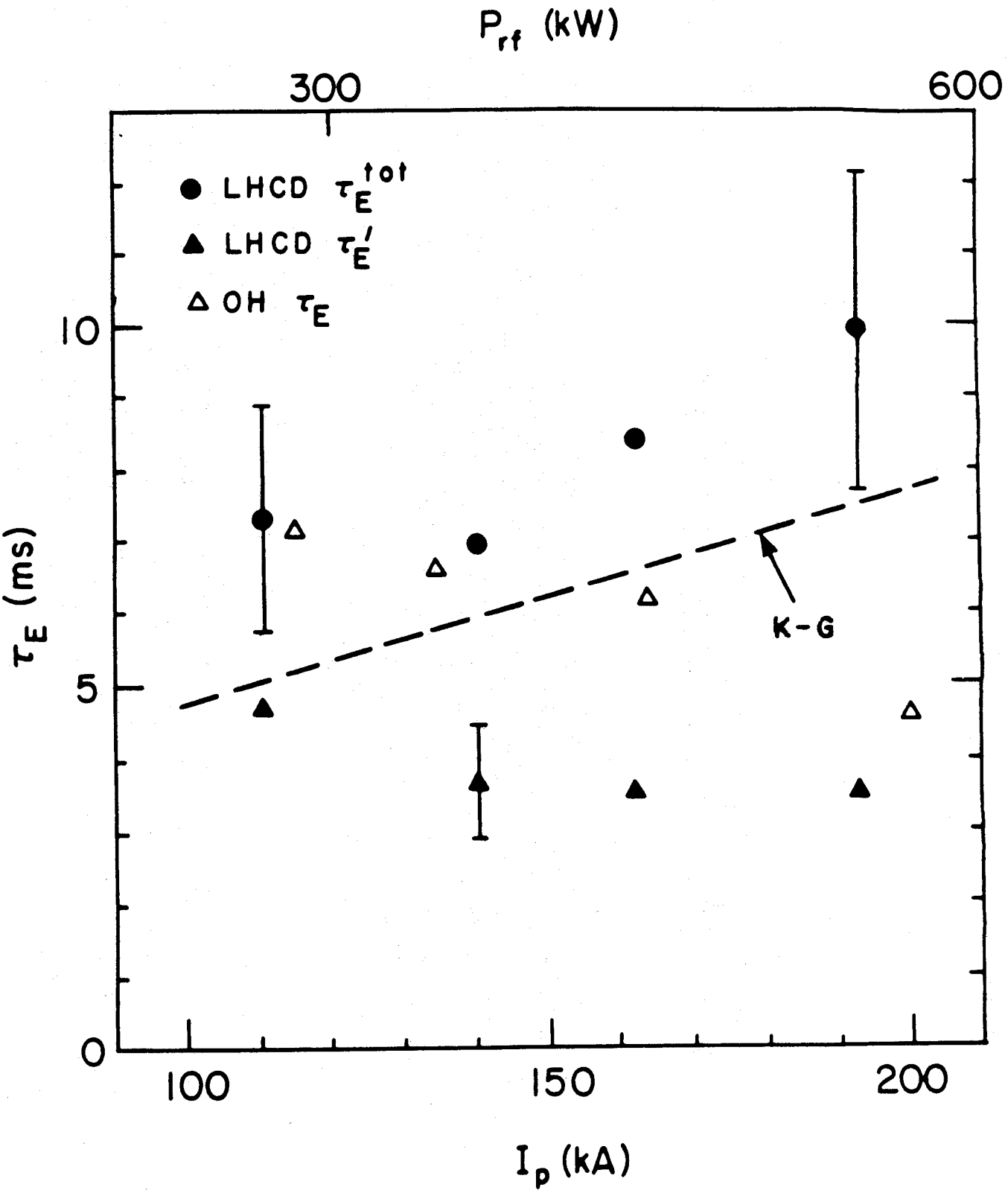
P_{rf} (kW)
300
600
● LHCD τ_E^{tot}
▲ LHCD τ_E'
△ OH τ_E
10
5
0
τ_E (ms)
K-G
100
150
200
I_p (kA)

Fig. 11

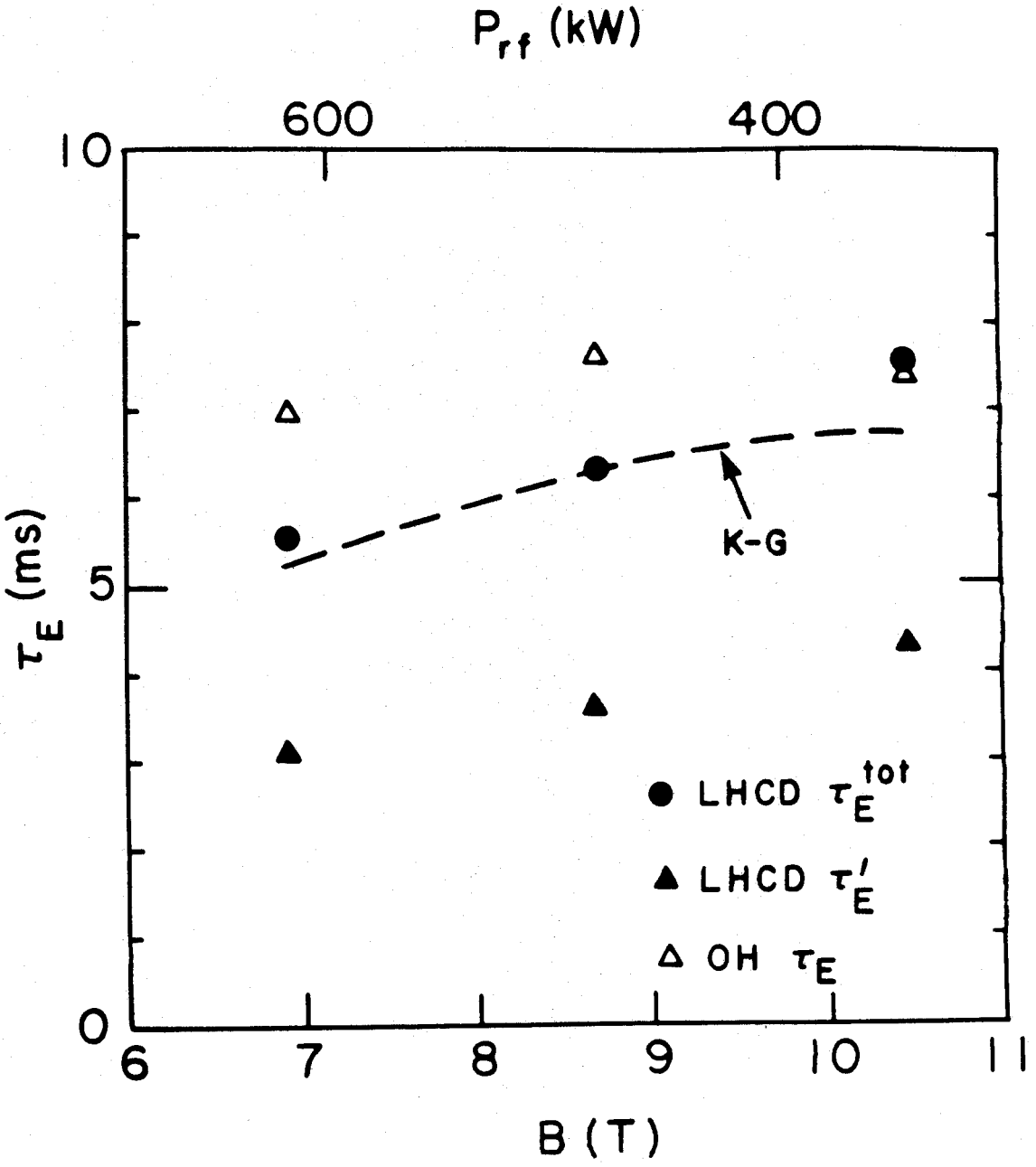
P_{rf} (kW)
600
400
10
5
0
τ_E (ms)
K-G
LHCD τ_E^{tot}
LHCD τ_E'
OH τ_E
6
7
8
9
10
11
B (T)

Fig. 12

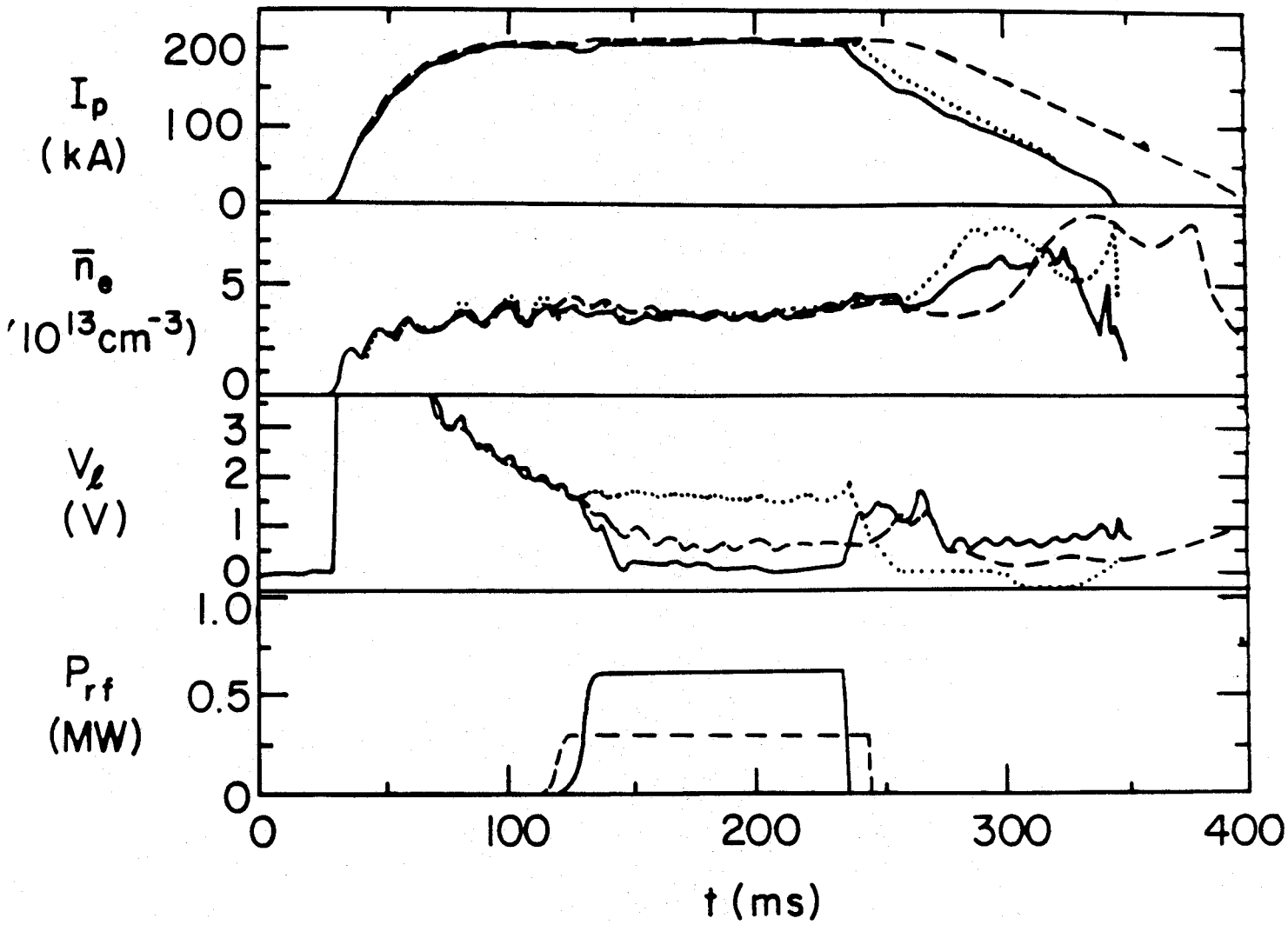
200
100
0
I_p
(kA)
5
0
$\bar{n}_e$
$(10^{13}cm^{-3})$
3
2
1
0
V_ℓ
(V)
1.0
0.5
0
P_{rf}
(MW)
0
100
200
300
400
t (ms)

Fig. 13

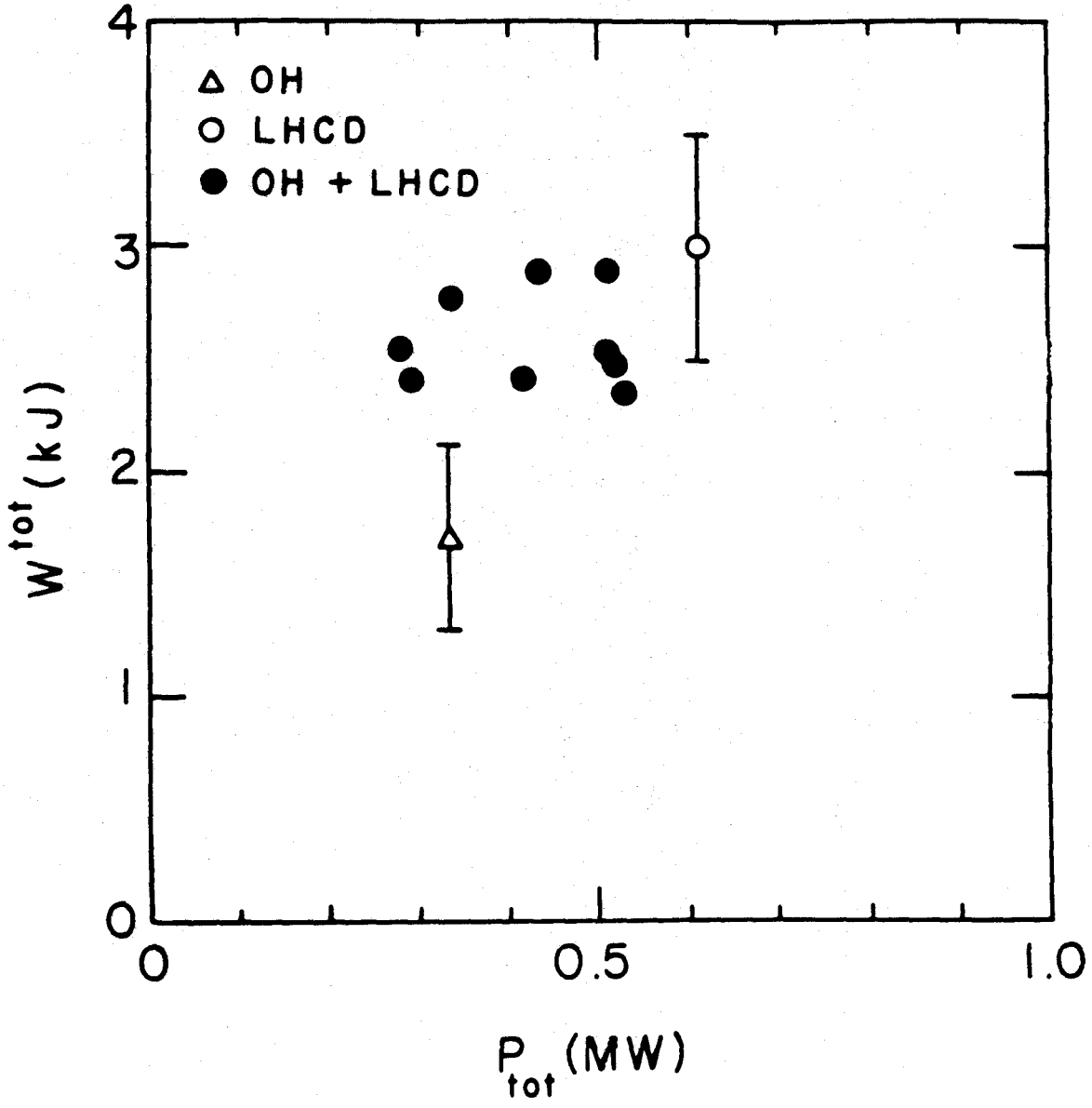

Fig. 14

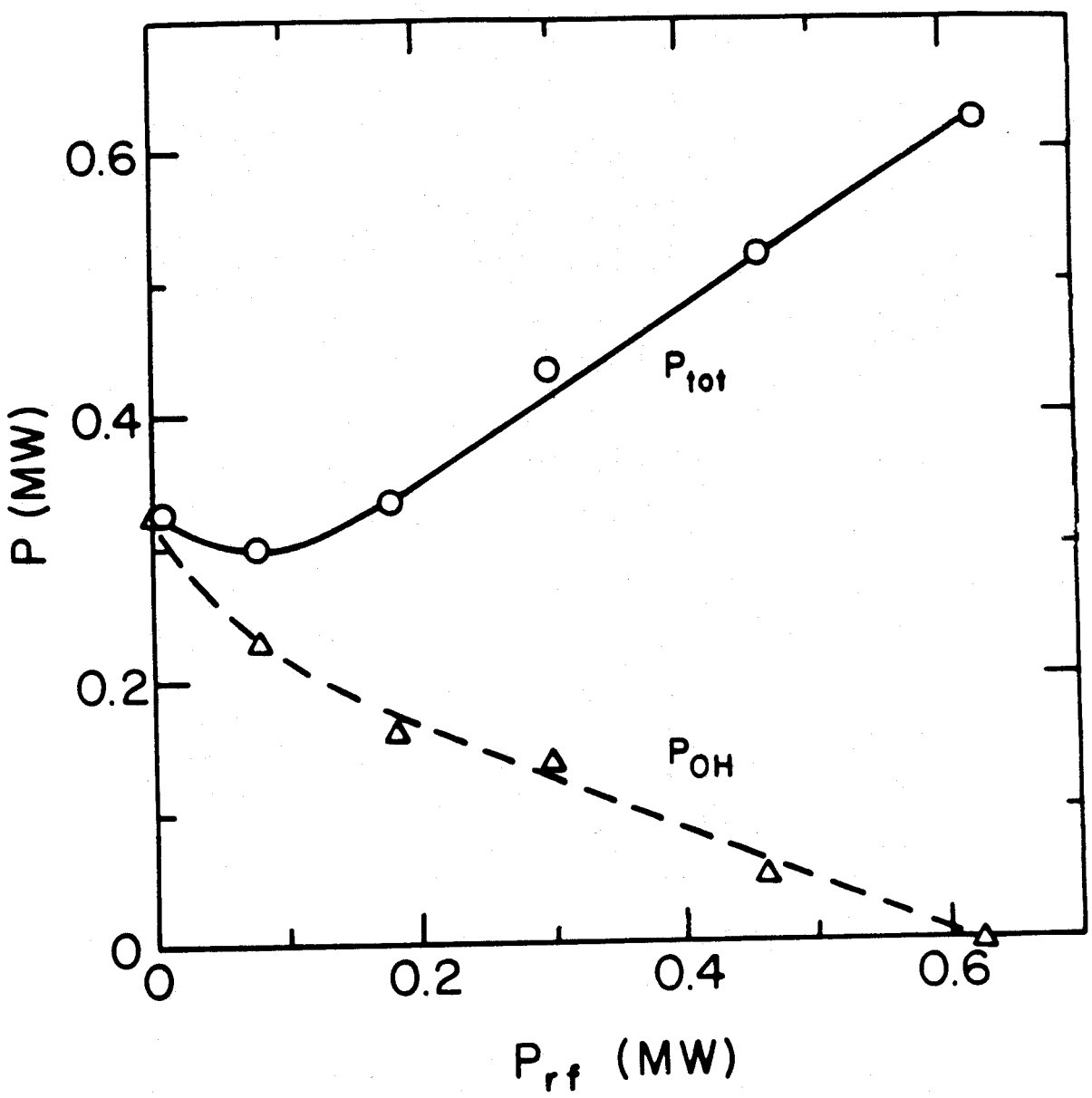

Fig. 15

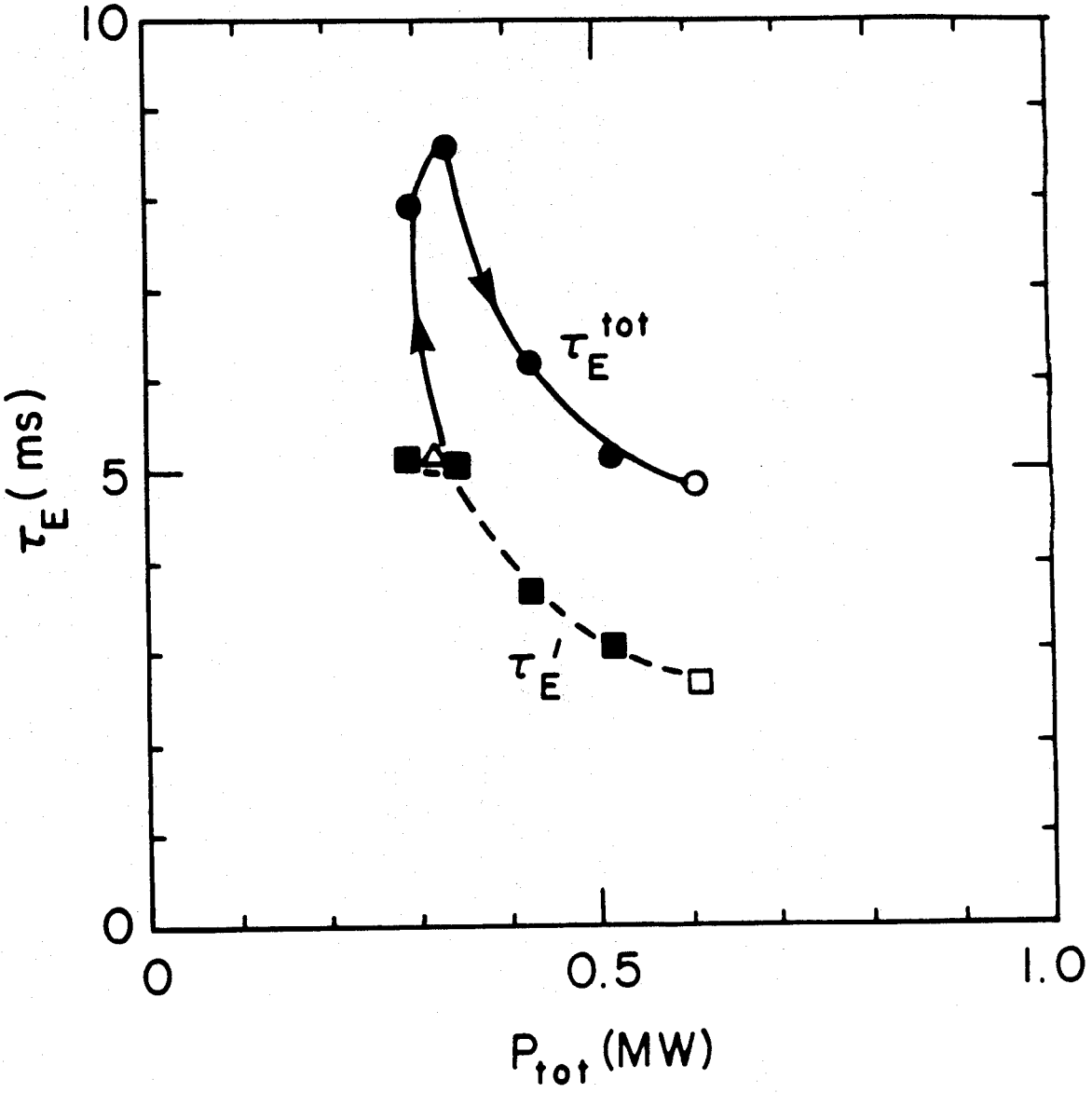

Fig. 16

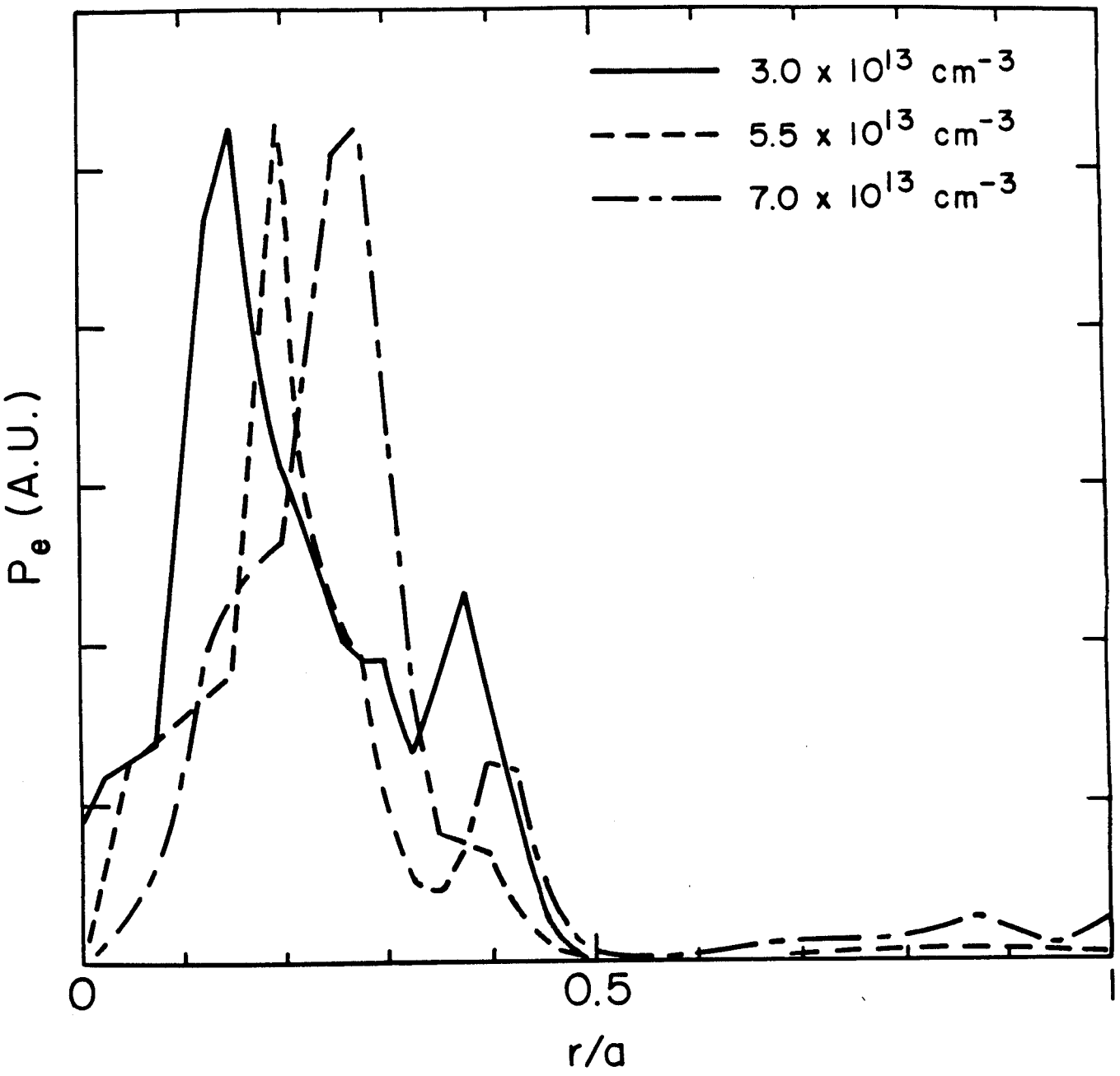

Fig. 17